1990      Thesis/Dissertation

A Statistical Survey of Electron Pitch Angle Distributions
in the Nightside Central Plasma Sheet
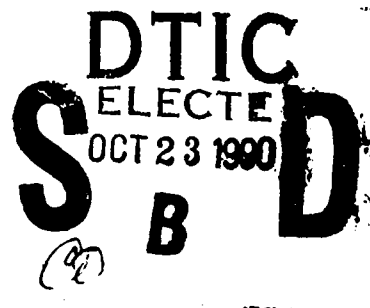
Timothy F. Alsruhe

AFIT Student at: University of California Los Angeles      AFIT/CI/CIA - 90-077

AFIT/CI
Wright-Patterson AFB OH 45433

86

UNCLASSIFIED

UNIVERSITY OF CALIFORNIA

Los Angeles

A Statistical Survey of Electron Pitch Angle Distributions

in the Nightside Central Plasma Sheet

A thesis submitted in partial satisfaction of the

requirements for the Degree Master of Science

in Atmospheric Sciences

by

Timothy F. Alsruhe

1990

For my Father,

L. Henry Alsruhe,

to whose self-taught breadth of knowledge I aspire.

# TABLE OF CONTENTS

## LIST OF FIGURES

## LIST OF TABLES

# ACKNOWLEDGMENTS

# ABSTRACT OF THE THESIS

## A Statistical Survey of Electron Pitch Angle Distributions
## in the Nightside Central Plasma Sheet

by

Timothy F. Alsruhe

Master of Science in Atmospheric Sciences

University of California, Los Angeles, 1990

S. V. Venkateswaran, Chair

The diffuse aurora is produced by precipitating electrons whose origin is believed to be the central plasma sheet. The process by which these electrons are continually scattered into the atmospheric loss cone is apparently unresolved. Arguments included processes which cause pitch angle scattering at the strong diffusion limit. A survey of equatorial pitch angle distributions of ~0.2-20KeV electrons has been conducted to determine the extent of pitch angle diffusion. Pitch angle distributions have been binned by location and geomagnetic activity for the nightside near earth plasma sheet. The average pitch angle anisotropy has been determined for each bin. Representative samples were selected from the bins of geomagnetically quiet ($Kp \leq 3$) distributions. The rate of diffusion was estimated by fitting distributions to plots of theoretically diffused distributions. Of the three energies examined (1.09, 4.52, 19.4keV), only distributions consistent with moderate to weak diffusion were observed. Even test cases of entirely isotropic distributions were consistent with only moderate diffusion. These results lead me to conclude that strong diffusion is usually not

in effect in the quiet near earth plasma sheet. Electron Cyclotron Harmonic (ECH) waves at the 3/2 harmonic have been suggested as the scattering mechanism responsible for maintaining the diffuse aurora. The necessary ECH wave amplitudes required to recreate average distributions were calculated. Derived amplitudes were one to three orders of magnitude greater than those amplitudes observed. Thus, it is concluded ECH do not occur with the frequency and amplitude necessary to sustain the continuous diffuse aurora.

# CHAPTER 1

# INTRODUCTION

The magnetosphere as a conduit for solar particles entering the earth's ionosphere is well established. It is generally agreed the source of the ionosphere's diffuse aurora is the near earth central plasma sheet [Lui et al., 1977; Meng et al., 1979]. The process by which electrons are scattered into the atmospheric loss cone and precipitated in the diffuse aurora is still a source of controversy. Kennel et al. [1970] first suggested electron cyclotron harmonic (ECH) waves as a mechanism for scattering electrons at the strong pitch angle diffusion limit. Lyons [1974] derived the ECH wave emissions necessary to put plasma sheet electrons on strong diffusion. Subsequent wave observations did not find adequate occurrences of ECH waves with sufficient amplitude to maintain the continuous diffuse aurora [Belmont et al., 1983; Roeder and Koons, 1989].

In this thesis, I present a survey of electron pitch angle distributions in the nightside central plasma sheet. The purpose of this survey is to determine the extent of pitch angle diffusion and the necessary ECH wave emissions required to produce observed distributions. Data points are sorted into various binning arrangements based on geographical location and geomagnetic activity. Statistically significant electron pitch angle anisotropies from each bin are selected and used to calculate the diffusion and required wave emissions.

Chapter 2 contains a description of the diffuse aurora and inner edge of the plasma sheet as well as a chronology of relevant theories and observations. In Chapter 3, the theories and processes of pitch angle diffusion and wave particle interactions are outlined. The particle detector and spacecraft which provided the data used in this research are describe in Chapter 4. Data selection, analysis, and observations, including sources of ambiguity and statistical uncertainties, are discussed in Chapter 5. Conclusions and areas

for future research are contained in Chapter 6.

# CHAPTER 2

# BACKGROUND

## 2.1 THE DIFFUSE AURORA

The diffuse aurora is a broad band of steady auroral glow that exists continually on the auroral oval. The diffuse aurora illumination is produced primarily by precipitating electrons. Mende and Eather [1976] estimate that less than 30% of the light is produced by protons. The diffuse aurora is a constant feature and is present at all levels of geomagnetic activity. It is the bright arc structure of the discrete aurora that the casual observer refers to as the "aurora". Unlike the discrete aurora, the diffuse aurora is not readily detected by the human eye. Its true immensity is only revealed by sensitive spaceborne photometric devices and charged particle detectors. Despite its mundane appearance, the diffuse aurora is the powerhouse of auroral phenomena, generating 80% of the total energy input into the polar region at solar maximum and no less then 50% at solar minimum [Whalen, 1985].

This paper concentrates exclusively on electron precipitation on the nightside. The general spectral range for electrons that are the primary cause of the diffuse aurora lies between a few hundred electron volts (eV) and ~10keV. Hardy et al. [1985] computed the total hemispheric electron energy flux as varying from $9.98 \times 10^{15}$ergs/s ster at Kp=1 to $2.06 \times 10^{17}$ergs/s ster for Kp≥6-. The total hemispheric electron number flux varies from $9.4 \times 10^{25}$el/s ster at Kp=0 to $6.41 \times 10^{26}$el/s ster for Kp ≥6-. This number flux can be misleading since 73-90% of the energy flux is carried by only a small number of electrons whose energies are greater than 660eV. The number flux of these electrons is $1.26 \times 10^{25}$el/s ster at Kp=0 to only $1.9 \times 10^{26}$el/s ster at Kp≥6-.. Contributions by particles greater than 10keV decrease smoothly [Meng et al. 1979; Kennel and Ashour-Abdalla, 1982; Lyons and Fennell, 1986]. Discussion in the literature of the pitch angle diffusion in the magnetic quiescent diffuse aurora is usually in the context of describing other more

3

dynamic auroral phenomena [Winningham, 1975; McDiarmid and Budzinski, 1968; Chase, 1968]. What can be gleaned from these observations is that the electron precipitation creating the diffuse aurora is usually isotropic or nearly isotropic in pitch angle. This isotropy has lead investigators to assume a filled atmospheric loss cone in the plasma sheet. Kennel [1969] notes a filled loss cone as an indication of strong diffusion (discussed in detail in Chapter 3).

On the nightside, the diffuse aurora extends from dusk to dawn in a band several hundred kilometers wide. The poleward edge of this aurora is weakly defined. Lui and Anger [1973] determined a globally average boundary location of 68°. The equatorial edge of the diffuse aurora varies as a function of geomagnetic activity [Gussenhoven et al., 1981,1983 and references therein]. The equatorward boundary is highly correlated to variations in the Kp index. This is particularly true on the nightside. Gussenhoven et al. [1981] found the minimum nightside equatorward boundary to be ~71° at 1800MLT in quiet times (Kp = 0). The boundary's maximum extent during geomagnetically active times reaches 57° at 0300 MLT for Kp = 5.

Since the flux of electrons into the diffuse aurora is approximately twice that of ions, the charge imbalance would be expected to create parallel electric currents. But any incipient parallel current is neutralized by a combination of cold ionospheric electrons scattered onto magnetic field lines by incoming magnetospheric electrons and by backscattered magnetospheric electrons. Energies of secondary and backscattered electrons range between a hundred eV and a few keV. When parallel electric currents do occur on field lines they accelerate electrons to create discrete structure in the aurora. Evidence of acceleration is a peak in the electron distribution. Though both the discrete and diffuse auroral particles share a common source -- the plasma sheet, the diffuse aurora is defined as the precipitation of unaccelerated particles and no peak in the distribution is observed.

Similarities in the diffuse aurora and the plasma sheet energy spectrum lead

4

numerous researchers to conclude a connection between the two regions [Winningham et al., 1975, Eather et al., 1976, Lui, 1977, Meng et al., 1979, Slater et al., 1980; Howitz et al., 1982]. Meng et al. [1979], the most widely referenced study on this connection, examined observations from the low orbiting DMSP satellite just above the diffuse aurora and ATS 6 satellite in the equatorial plasma sheet. Simultaneous observations taken by these satellites when on conjugate field lines produced nearly identical electron spectra.

## 2.2 THE PLASMA SHEET

The boundaries of the inner edge of the plasma sheet are more easily observed than explained. Gussenhoven et al. [1981] projected the equatorward boundary of the auroral oval back onto the magnetic equatorial plane. They found the latitudial extent of the inner edge varies in local time and is approximately related to the Kp index. Mapping these boundaries to field lines in the equatorial plane, the inner edge ranged from a minimum of 3.5 earth radii (Re) at 0300MLT for Kp = 5 to a maximum of 10.2Re at 2100MLT for Kp = 0.

Two theories predominate on what process is responsible for defining the inner edge of the plasma sheet. One theory is based on pitch angle diffusion [Kennel, 1969; Ashour-Abdalla and Thorne, 1978] and the other on single particle motion [Kivelson and Southwood, 1975; Ejiri, 1978; Southwood and Kaye, 1979; among others]. Both theories assume convection due to the cross tail electric field will renew the plasma sheet of particles lost to precipitation.

The strong pitch angle diffusion theory is based on the assumption particle lifetimes approach the strong pitch angle diffusion limit (detailed in Chapter 3). This facilitates an isotropic pitch angle distribution where the particle lifetimes $\tau$ approach a minimum [Kennel and Ashour-Abdalla, 1982].

5

$$\tau_m = \frac{2\tau_{1/4B}}{\alpha_L^2} \tag{2-1}$$

where $\tau_{1/4B}$ is the quarter bounce period (i.e. between the equator and the atmosphere) and $\alpha_L$ is the width of the equatorial loss cone.

As particles convect toward the earth from the magnetotail few particles are lost from the flux tubes. This is a consequence of the electron minimum lifetime $\tau_m$ being much longer than characteristic flow time $\tau_f$ at great distances. In a dipole field,

$$\tau_m \sim \frac{L^4}{E_e^{1/2}} \tag{2-2}$$

where $E_e$ is the electron energy and L is the distance from the earth in a dipole magnetic field measured in Re. L is known as the McIlwain parameter [McIlwain, 1961]. The characteristic flow time is

$$\tau_f = \frac{10^7}{L\phi^2} \tag{2-3}$$

where $\phi$ is the electric potential across the magnetotail.

Closer to the earth the magnetic flux tubes decrease in volume, thus increasing the flux density. In (2-2), $E_e$ changes with L adiabatically so that finally, for characteristic electron energies at small L (i.e. $\leq$ 7-10Re), $\tau_m$ is smaller than the characteristic $\tau_f$. At this point electrons rapidly precipitate [Kennel and Ashour-Abdalla, 1982]. Due to their mass, protons would be expected to have longer lifetimes and the inner edge of the plasma sheet should be closer to the earth. Yet, the electron inner edge is observed closer to the earth [Newell and Meng, 1987]. This is explained by Ashour-Abdalla and Thorne [1978] who suggest electron precipitation in regions of field aligned currents can create an environment in which ion cyclotron waves can pitch angle scatter ions. Though such ion cyclotron waves have been documented by Gurnett and Frank [1977] and, during substorms, by Cornwall and Schulz [1971], the connection to electron precipitation has not been confirmed.

The second theory on the formation of the inner edge of the plasma sheet is based

on the motion of single particles in a dipole magnetic field and a Stern-Volland cross tail electric field . No initial diffusion process is assumed. A model of the particle motion in the equatorial plane of the magnetosphere is given by the electrostatic potential [Roederer, 1970]. As electrons convect toward the earth, zero energy particles follow electric equipotentials that exclude them from the plasmapause. Higher energy electrons are affected by eastward magnetic drifts proportional to their energies. The larger the energy the farther from the earth the particle will be deflected. The lowest energy electrons will convect closest to the earth to form the inner edge of the plasma sheet. Since ions drift to the west they partially standoff the eastward corotational force. Ions should convect closer to the earth than equivalently energized electrons. This is usually not observed; the exception is at dusk [Newell and Meng, 1987]. In this theory, precipitation of electrons into the diffuse aurora would require a scattering mechanism such as waves.

Neither model of magnetotail convection is fully supported by observations. The convection of particles in the strong diffusion, as assumed in the first theory above, is not proven. Fairfield and Viñas [1983] suggest that the inner edge of the plasma sheet is a function of both theories.

## 2.3 RESEARCH CHRONOLOGY

A knowledge of the mean rate of diffusion is requisite in the determination of the primacy of ECH waves sustaining the diffuse aurora. In this work, I investigate the assumption of pitch angle scattering at the strong diffusion limit. This is done by comparing observed pitch angle distributions to those theoretically derived from this limit. The ECH wave amplitudes necessary to create the observed distributions in this study are computed. These amplitudes are then compared to the ECH wave observations of Roeder and Koons [1989] and Belmont et al. [1983]. This thesis is another step in a series of studies dating back to Kennel et al. [1970].

The Ogo 5 satellite, launched in March 1968, observed several new types of magnetospheric electric field emissions with wave frequencies $\omega$ above the local electron cyclotron frequency $\Omega_-$. The most common of these waves have become known as Electron Cyclotron Harmonic (ECH) waves because of its tendency to occur at odd half multiples of $\Omega_-$. Kennel et al. [1970] named ECH waves as a likely source of pitch angle diffusion and turbulent energization of auroral zone electrons. They cited the fact that ECH waves with $\omega \geq 3\Omega_-/2$ are observed near the geomagnetic equator on field lines anchored in the auroral region and typically have intensities of 1-10mV/m. Lyons [1974], using quasi-linear diffusion theory, showed that these waves should generally cause strong pitch angle diffusion of electrons of a few tenths keV to a few keV. Lyons noted that the most intense waves could put electrons of energies up to ~100keV on strong diffusion. The work of Kennel et al. [1970] and Lyons [1974] is the theoretical basis to which all observational surveys of the plasma sheet have since been compared.

Continued analysis of OGO 5 data [Fredricks and Scarf, 1973] and new data available from GEOS 1 and GEOS 2 [Gough et al., 1979; Canu, 1982] afforded better definition of the location, intensity, and frequency of occurrence of ECH waves. It was noted the waves were more closely concentrated on the geomagnetic equator than had originally been suggested. The observations from GEOS indicated intense ECH waves did not commonly occur [Gough et al., 1981].

Belmont et al. [1983] refined Lyons' [1974] theoretical calculations by adapting new information derived by Gough et al. [1979,1981] and Canu [1982]. Wave interactions were confined to within a few degrees of the magnetic equator, instead of assuming interaction along the entire field line. A minimum wave amplitude required to place a resonant 1keV electron on strong diffusion was determined to be in excess of 2mV/m. Belmont et al. found amplitudes of 2mV/m were observed only 9% of the time when GEOS was closest to the magnetic equator and only 1% of the time at -3° off the

8

equator. The paucity of ECH waves with adequate amplitudes implies they are not the single (or even the primary) mechanism for putting 1keV electrons on strong diffusion

Fairfield and Viñas [1984] concluded pitch angle diffusion does not occur at the strong diffusion rate in the plasma sheet. They based their conclusions on two observations. First, the inner edge of the plasma sheet was too close to the plamapause. Had electrons been on strong diffusion they would have been lost sooner and the inner edge of the plasma sheet would stand farther out. The second observation was of "frequent and persistent occurrences of anisotropies [in the electron distributions]." Fairfield and Viñas suggested that under the influence of strong diffusion these anisotropies would be smoothed. Thus, they support the single particle theory for the convection of electrons. This theory would cause electrons normal to the magnetic field to be energized more than field aligned particles. The longer a particle distribution remains under the influence of the convection electric field in a dipole magnetic field the greater the pitch angle anisotropy.

The electron distributions studied by Schumaker et al. [1989] did not support strong diffusion by ECH waves either. Though the distributions were isotropic in the loss cone, immediately outside the loss cone they become anisotropic. This type of distribution would require the diffusion coefficient to be large across the loss cone and then decrease toward higher pitch angles. This is contrary to the altitude normalized diffusion coefficient calculations of Lyons [1974]. Lyons' calculations showed pitch angle diffusion coefficients peak well away from $\alpha = 0°$ and decreases towards $\alpha = 0°$ (see Fig. 3-3). The diffusion coefficient discrepancy notwithstanding, ECH wave amplitudes great enough to produce the distributions recorded by Schumaker et al. have still not been observed.

Roeder and Koons [1989] conducted a survey of ECH emissions using AMPTE and SCATHA data at ±10° and ±5° of the geomagnetic equator, respectively. They found that even in the region of maximum ECH emissions (i.e., 0300-0600MLT, 4-8 Re) amplitudes exceeding 0.012mV/m were observed only 60% of the time. Amplitudes of

9

0.035mV/m were observed only 25% of the time. Roeder and Koons concluded the occurrence and amplitude of ECH waves were too small to create the necessary pitch angle diffusion to account for the continuous diffuse auroral. This conclusion supported the earlier work of Belmont et al.

# PITCH ANGLE DIFFUSION

## 3.1 ATMOSPHERIC LOSS CONE

Particles in a magnetic mirror can be characterized as precipitating or trapped depending on their location in velocity space. A trapped particle mirrors on a field line described by

$$\sin^2 \alpha_0 = \frac{B_o}{B_m} \qquad (3\text{-}1)$$

where $\alpha_0$ is the equatorial pitch angle, $B_o$ is the magnetic field strength at the equator (the weakest strength on a field line), and $B_m$ is the mirror point field strength.

Precipitating particles do not mirror on their respective field lines before entering the earth's atmosphere and collide with ionospheric particles. The range of pitch angles at the equator who's mirror point is within the earth's atmosphere is defined as the atmospheric loss cone $\alpha_L$. The height of the earth's atmosphere dense enough to significantly increase the probability of collision is nominally 100km. The atmospheric loss cone is given by

$$\alpha_L = \arcsin \left(\frac{B_o}{B_{100}}\right)^{1/2} \qquad (3\text{-}2)$$

where $B_{100}$ is the magnetic field strength at 100km. The loss cone width is independent of particle energy, but there is still a particle species dependance. The larger cross-section of protons increases their probability of collision at altitudes higher than electrons thus giving them a wider loss cone.

A bounce period $\tau_B$ is defined as the time necessary for a particle to travel from the equator, mirror in both hemispheres, and return to the equator. Particles with equatorial pitch angles $\alpha_0$ less than or equal to the loss cone angle are precipitated into the atmosphere within a quarter bounce period $\tau_{1/4B}$ (i.e. lost between the equator and the first mirror point). Particle lifetimes $\tau_L$ are

11

$$\tau_L = \tau_{1/4B} \quad \text{for } \alpha_o \leq \alpha_L \tag{3-3}$$

$$\tau_L = \infty \quad \text{for } \alpha_o > \alpha_L \tag{3-4}$$

Equation (3-3) defines loss cone particles and (3-4) defines trapped particles. Trapped particles in the plasma sheet are more correctly called quasi-trapped. The are trapped until such time as they are lost from the magnetosphere or scattered into the loss cone.

## 3.2 ADIABATIC INVARIANTS

Three periodic motions arise from trapped particles; gyration, bounce and drift. The first and fastest motion is a particle's gyration about a magnetic field line. The second motion is the periodicity associated with a particle's bounce between mirror points. The third and slowest motion is the azimuthal drift around the earth. If the particle moves slowly through variations in the magnetic field these periods are conserved.

Conservation of the magnetic moment by a particle's gyromotion is called the first adiabatic invariant and is defined

$$\mu = \frac{mV_\perp^2}{2B} = \frac{p_\perp^2}{2Bm} = \frac{E \sin^2\alpha}{B} \tag{3-5}$$

where m is the mass, $V_\perp$ is the particle velocity, $p_\perp$ is the momentum, both $V_\perp$ and $p_\perp$ are normal to the magnetic field, E is the particle energy, and $\alpha$ is the pitch angle. The second adiabatic invariant is the relationship of a particle's bounce motion on field lines

$$J = \int p_{||} \, dl \tag{3-6}$$

where $p_{||}$ is the parallel component of the momentum and l is the field line length from the equator. Conservation of the magnetic flux in a particle's drift motion is defined as the third adiabatic invariant

$$\Phi = \int B \, dA \tag{3-7}$$

12

where **A** is the area within the drift orbit.

## 3.3 PITCH ANGLE DIFFUSION

Processes that violate either the first or second adiabatic invariant can scatter, or diffuse, quasi-trapped particles to lower equatorial pitch angles and eventually into the loss cone. Variations in electric or magnetic fields or interaction with magnetospheric waves can cause such diffusion. Here we will concentrate on wave-particle interactions.

Diffusion in velocity space due to resonant waves interacting with particles is a combination of pitch angle and energy diffusion.

$$D_{\alpha\alpha} = \frac{(\Delta\alpha)^2}{2\tau_B} \tag{3-8}$$

$$D_{EE} = \frac{(\Delta E)^2}{E^2 \, 2\tau_B} \tag{3-9}$$

where D is the diffusion coefficient, $\Delta\alpha$ and $\Delta E$ are the small changes in pitch angle and energy, respectively. A simplifying argument we will assume is that a particle's random walk in energy diffusion is much slower than in pitch angle ($D_{\alpha\alpha} \gg D_{EE}$). The reasons for making this assumption is the invocation of $3/2\Omega_-$ ECH waves in Section 3-5. Kennel [1969] states it is not inappropriate to disregard the energy diffusion and examine only pitch angle diffusion for the small phase velocity of electrostatic $3/2\Omega_-$ ECH waves.

The time it takes a particle to diffuse across the loss cone in a quarter bounce period represents the separation of strong and weak diffusion. In weak diffusion, particles will fail to completely diffuse across the loss cone in a quarter bounce period and are precipitated.

$$\frac{\alpha_L^2}{D_{\alpha\alpha} \, \tau_{1/4B}} \gg 1 \tag{3-10}$$

$$\tau_D \gg \tau_{1/4B} \tag{3-11}$$

where $\tau_D$ is diffusion time. The weaker $D_{\alpha\alpha}$, the weaker the flux in the loss cone. In very weak diffusion the loss cone is virtually empty.

13

In strong diffusion, particles can be diffused into and out of the loss cone in a quarter bounce period.

$$\frac{\alpha_L^2}{D_{\alpha\alpha}\, \tau_{1/4B}} \ll 1 \tag{3-12}$$

$$\tau_D \ll \tau_{1/4B} \tag{3-13}$$

The loss cone remains filled in strong diffusion since precipitated particles are immediately replaced.

Figure 3-1 is an enlightening analogy to the levels of pitch angle diffusion as illustrated by Kennel et al. [1969] (originally formalized by O'Brian [1964]). The pump represents the source of particles, the water level in the bucket represents the quasi-trapped flux intensity, the spout is analogous to the loss cone. In 3-1a., the steady state case is shown where weak diffusion balances injection and precipitation. The source in this case determines the loss rate to atmosphere. Strong particle injections are represented in 3-1b. Here the pump overwhelms the spout's removal capacity. The spout (loss cone) regulates the rate of loss.

## 3.4 PITCH ANGLE DISTRIBUTIONS

The distribution of particle pitch angles is described by the Fokker-Plank equation

$$\frac{\partial f}{\partial t} - \frac{1}{\sin\alpha}\,\left(D_{\alpha\alpha}\, \sin\alpha\, \frac{\partial f}{\partial\alpha}\right) = S(\alpha,E) - L(\alpha,E) \tag{3-14}$$

where $f(x,v,t)$ is the one particle (Vlasov) distribution function in velocity space, $S(\alpha,E)$ represents sources, and $L(\alpha,E)$ are sinks in pitch angle and energy.

Emulating Kennel and Petschek [1966], we will solve for the pitch angle distribution assuming a steady state diffusion solution. Two preliminary solutions will be required; one inside the loss cone and one outside. These solutions take into account differences in sources and sinks.

14

WEAK DIFFUSION
40 KEV ELECTRONS
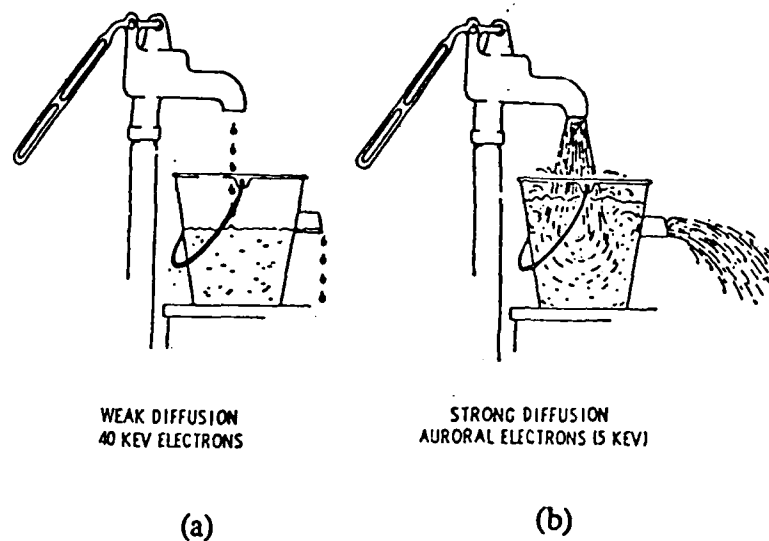
STRONG DIFFUSION
AURORAL ELECTRONS (5 KEV)

(a)

(b)

Figure 3-1. Leaky bucket. (a) In weak diffusion, particles precipitate at the rate they are added. A steady state is obtained. (b) In strong diffusion, the precipitation mechanism saturates due to the finite size of the loss cone. [From Kennel, 1969]

First, solve for the distribution in the loss cone where we assume no sources $(S(\alpha,E) = 0)$. The particle sink in the loss cone is

$$L = \frac{f}{\tau_L} = \frac{f}{\tau_{1/4B}} \tag{3-15}$$

From (3-14) steady state diffusion in the loss cone becomes

$$\frac{1}{\alpha} \frac{\partial}{\partial \alpha} \left( D_{\alpha\alpha} \ \alpha \ \frac{\partial f}{\partial \alpha} \right) - \frac{f}{\tau_{1/4B}} = 0 \tag{3-16}$$

where the law of small angles is used for $\alpha$

Applying the assumption of $D_{\alpha\alpha} \gg D_{EE}$, the pitch angle distribution in the loss cone is considered independent of time and can be expressed

$$g(\alpha) \sim X(E) \ I_o \frac{\alpha}{(D_{\alpha\alpha} \ \tau_{1/4B})^{1/2}} \tag{3-17}$$

where $I_o$ is a modified Bessel function and $X(E)$ is an arbitrary function.

Outside the loss cone $(\alpha > \alpha_L)$ there are no sinks and the steady state diffusion equation (3-14) is

$$\frac{1}{\sin \alpha} \frac{d}{d\alpha} \left( D \sin \alpha \ \frac{df}{d\alpha} \right) = S(\alpha,E) \tag{3-18}$$

where $S(\alpha,E)$ is the source flux of the distribution. In steady state, the source flux will equal the precipitation flux. Kennel and Petschek [1966] make the following simplifying assumption; particles are injected only at flat pitch angles (i.e. $\pi/2$) and the diffusion flux is constant at any angle $\alpha < \pi/2$ and is equal to $S(\alpha,E)$. The source flux can be broken into components of energy and pitch angle, $S(\alpha,E) = S^*(E) \ S(\alpha - \pi/2)$. The flat pitch angle assumption requires $S(\alpha) = 0$ everywhere except at $\alpha = \pi/2$.

The equation of the distribution function exterior to the loss cone which satisfies (3-14) is

$$D^* \tan \alpha \frac{\partial f}{\partial \alpha} = \int_0^{\pi/2} \sin \alpha \ S(\alpha - \frac{\pi}{2}) \ S^*(E) \ d\alpha \tag{3-19}$$

$$= S^*(E)$$

where $D = D^*/\cos \alpha$. Equation (3-19) quantifies the assumption that the source strength on the right side of the equation is balanced by the diffusion flux on the left.

Integrating to solve for f yields,

$$f(\alpha) = \frac{S^*(E)}{D^*} \ln (\sin \alpha) + Z_o \qquad (3-20)$$

where $Z_o$ is a constant of integration.

If $f(\alpha)$ and the diffusion flux are considered continuous, then matching the loss cone distribution (3-17) with the external distribution (3-20) will eliminate $X(E)$ and $Z_o$. The complete exterior distribution, symmetric about $\alpha = \pi/2$ is then

$$f(\alpha,E) = \frac{S^*(E)}{D^*} \left( h(\alpha_o) + \ln \left( \frac{\sin \alpha}{\sin \alpha_L} \right) \right) \qquad (3-21)$$

where $h(\alpha_o)$ is the loss cone solution

$$h(\alpha) = \frac{(D^* \tau_{1/4B})^{1/2}}{\alpha_L} \frac{I_o \left( \frac{\alpha}{(D^* \tau_{1/4B})^{1/2}} \right)}{I_1 \left( \frac{\alpha_o}{(D^* \tau_{1/4B})^{1/2}} \right)} \qquad (3-22)$$

The lifetime for trapped particles is equal to the total number of trapped particles divided by the particle loss rate. Recall from (3-19), $S^*(E)$ is equivalent to the precipitation flux in the loss cone. Dividing the exterior distribution (3-21) by $S^*(E)$ yields

$$\tau_L = \frac{1}{D^*} \int_{\alpha_L}^{\pi/2} \sin \alpha \left( h(\alpha_o) + \ln \left( \frac{\sin \alpha}{\sin \alpha_o} \right) \right) \qquad (3-23)$$

$$= \frac{1}{D^*} \left( h(\alpha_o) - \ln \frac{q \tan \alpha_o}{2} \right)$$

where q is the charge.

Observed particle pitch angle distributions in weak diffusion are highly anisotropic across the loss cone. Quantitatively, this is bore out in the asymptotic representation of the Bessel function where the loss cone distribution increases exponentially from the center ($\alpha = 0$) to the edge ($\alpha = \alpha_o$).

In weak diffusion,

$$I_o(z) \sim \frac{q^z}{(2\pi z)^{1/2}} \sim I_1(z) \qquad (3\text{-}24)$$

where z represents

$$z = \frac{\alpha_o}{(D^* \tau_{1/4B})^{1/2}} \gg 1 \qquad (3\text{-}25)$$

so then (3-22) becomes

$$h(\alpha) \sim \frac{(D^* \tau_{1/4B})^{1/2}}{\alpha_L} \ll 1 \qquad (3\text{-}26)$$

This effectively reduces quasi-trapped particles in weak diffusion (WD) to lifetimes of

$$\tau_{LWD} \Rightarrow \frac{1}{D^*} \ln\left(\frac{2}{q\alpha_L}\right) \qquad (3\text{-}27)$$

Note the lifetime is directly proportional to the diffusion rate and only logarithmically to the width of the loss cone.

Pitch angle distributions observed in strong diffusion are isotropic across the loss cone. Kennel and Petschek employ the small argument expansion of the Bessel function for strong diffusion ($z \ll 1$)

$$I_o(z) \Rightarrow 1 \qquad (3\text{-}28)$$

$$I_1(z) \sim z/2 \qquad (3\text{-}29)$$

Applying these results to (3-22)

$$h(\alpha) \approx \frac{2(D^* \tau_{1/4B})^{1/2}}{\alpha_L^2} \gg 1 \qquad (3\text{-}30)$$

The result is a strong diffusion (SD) minimum lifetime

$$\tau_{LSD} \Rightarrow \frac{2\tau_{1/4B}}{\alpha_o^2} = \tau_m \qquad (3\text{-}31)$$

A minimum lifetime $\tau_m$ sets an upper limit on the quasi-trapped particles' rate of removal. Note $\tau_m$ is controlled by the size of the loss cone and is independent of the strength of the diffusion coefficient D and charge q (i.e. particles can't be removed faster than $\tau_m$ regardless of the strength of the diffusion).

The Kennel and Petschek treatise on steady state diffusion is restrictive in that pitch angle scattering is limited to only one location on a field line, and their definition of $D_{\alpha\alpha} \sim$

$D^*/\cos\alpha$ is not representative in the magnetosphere. Lyons et al. [1972] calculated a time average D over an electron bounce period. This was defined by relating the local $D(\alpha)$ to the equivalent equatorial $D(\alpha_o)$. The bounce averaged equatorial pitch angle diffusion coefficient is

$$D(\alpha_o) = \frac{1}{\tau_B} \int_0^{\tau_B} D(\tau) \left(\frac{\partial\alpha_o}{\partial\alpha}\right)^2 dt \qquad (3\text{-}32)$$

Equation (3-32) can be transformed over magnetic latitude $\lambda$ to produce

$$D(E,L,\alpha_o) = \frac{1}{s(\alpha_o)} \int_0^{\lambda_m} D(\alpha)\ \frac{\cos\alpha}{\cos^2\alpha_o}\ \cos^7\lambda\ d\lambda \qquad (3\text{-}33)$$

where $\lambda_m$ is the mirror latitude, and $s(\alpha_o)$ is a correction for the variation in $\tau_B$ for a given $\alpha$ ($s(\alpha_o) = 1.38 - .032(\sin\alpha_o + \sin^{1/2}\alpha_o)$ [Schulz and Lanzerotti, 1973].

Next $f(x,v,t)$ is converted from velocity space to phase space $f(E,L,\alpha_o,t)$ by averaging (3-14) over an electron bounce in a dipole field.

$$\frac{\partial f_o}{\partial t} = \frac{1}{s(\alpha_o)\ \sin\alpha_o\ \cos\alpha_o}\ \frac{1}{\partial\alpha_o}\ s(\alpha_o)\ \sin(\alpha_o)\ \cos\alpha_o\ D(\alpha_o)\frac{\partial f_o}{\partial\alpha_o} - \frac{f_o}{\tau_{atm}} \qquad (3\text{-}34)$$

where $\tau_{atm} = \tau_{1/2B}$ (half bounce period) for $\alpha \le \alpha_o$ and $\tau_{atm} = \infty$ for $\alpha > \alpha_L$.

The steady state model is rarely seen in the magnetosphere. More common are electron injections on the order of minutes followed by several hours of decay. Roberts [1969] studied artificial injections by a nuclear explosions and natural injections and found they both soon decayed to a normal mode. Lyons used this fact to break the equatorial pitch angle distribution into

$$f_o(t,\alpha_o) = F(t)\ g(\alpha_o) \qquad (3\text{-}35)$$

where $F(t)$ denotes the equatorial density of particles for a given energy and $g(\alpha_o)$ denotes the shape of the distribution.

Substituting (3-35) into (3-34) produces

$$\left( \frac{1}{\tau_{atm}} + \frac{1}{F} \frac{\partial F}{\partial t} \right) g(\alpha_o)\, s(\alpha_o)\, \sin \alpha_o \cos \alpha_o$$

$$= \frac{\partial}{\partial \alpha_o} s(\alpha_o)\, \sin \alpha_o \cos \alpha_o\, D(\alpha_o) \frac{\partial g}{\partial \alpha_o} \tag{3-36}$$

Lyons converted (3-36) to integral form by carrying out the integration twice between 0 and $\pi/2$, specifying $\dfrac{\partial g}{\partial \alpha_o} = 0$ at $\alpha_o = 0°$ and $\alpha_o = 90°$. The resulting equatorial pitch angle distribution $g(\alpha_o)$ takes the form

$$\ln \frac{g(\alpha_o)}{g(0)} = \frac{2}{T_o} \int\limits_0^{\alpha_o} \frac{1}{g(\alpha')\, s(\alpha')\, \sin \alpha' \cos \alpha'\, D(\alpha')} \cdot$$

$$\left( \int\limits_0^{\alpha''} g(\alpha)\, \sin \alpha \cos \alpha\, d\alpha - \eta \int\limits_0^{\alpha'} g(\alpha) s(\alpha)\, \sin \alpha\, \cos \alpha\, d\alpha') \right) \tag{3-37}$$

where

$$\alpha'' = \alpha' \quad \text{for } \alpha' \le \alpha_L$$

$$\alpha'' = \alpha_L \quad \text{for } \alpha' > \alpha_L$$

and

$$\eta = \frac{\displaystyle\int\limits_0^{\alpha_L} g(\alpha_o)\, \sin \alpha \cos \alpha_o\, d\alpha_o}{\displaystyle\int\limits_0^{\pi/2} g(\alpha_o)\, s(\alpha_o)\, \sin \alpha_o \cos \alpha_o\, d\alpha_o} \tag{3-38}$$

Thus, the equatorial pitch angle distribution can be determined for given values of $D(\alpha_o)$.

The precipitation lifetime,

$$\tau_p = -\left( \frac{1}{F} \frac{\partial F}{\partial t} \right)^{-1} \tag{3-39}$$

is related to $g(\alpha_o)$ by

$$\tau_p = \frac{T_o}{2\eta} \tag{3-40}$$

Figure 3-2. Equatorial pitch angle distribution at $L = 2, 4,$ and 8. The results of (3-37) for $D(0°)\tau_m = 10^1, 10^0, 10^{-1},$ and $10^2$ where $D(0°)$ is the diffusion coefficient at $0°$ pitch angle and $\tau_m$ is the minimum lifetime for particles undergoing strong diffusion. For each value of $D(0°) \tau_m$, pitch angle distributions are shown for values of the diffusion coefficient at $90°$ given by $D(90°)/D(0°) = 10^2, 10^0,$ and $10^{-2}$. $D(\alpha_o)$ is assumed to vary linearly between $\alpha_o = 0°$ and $\alpha_o = 90°$. [From Lyons, 1973]
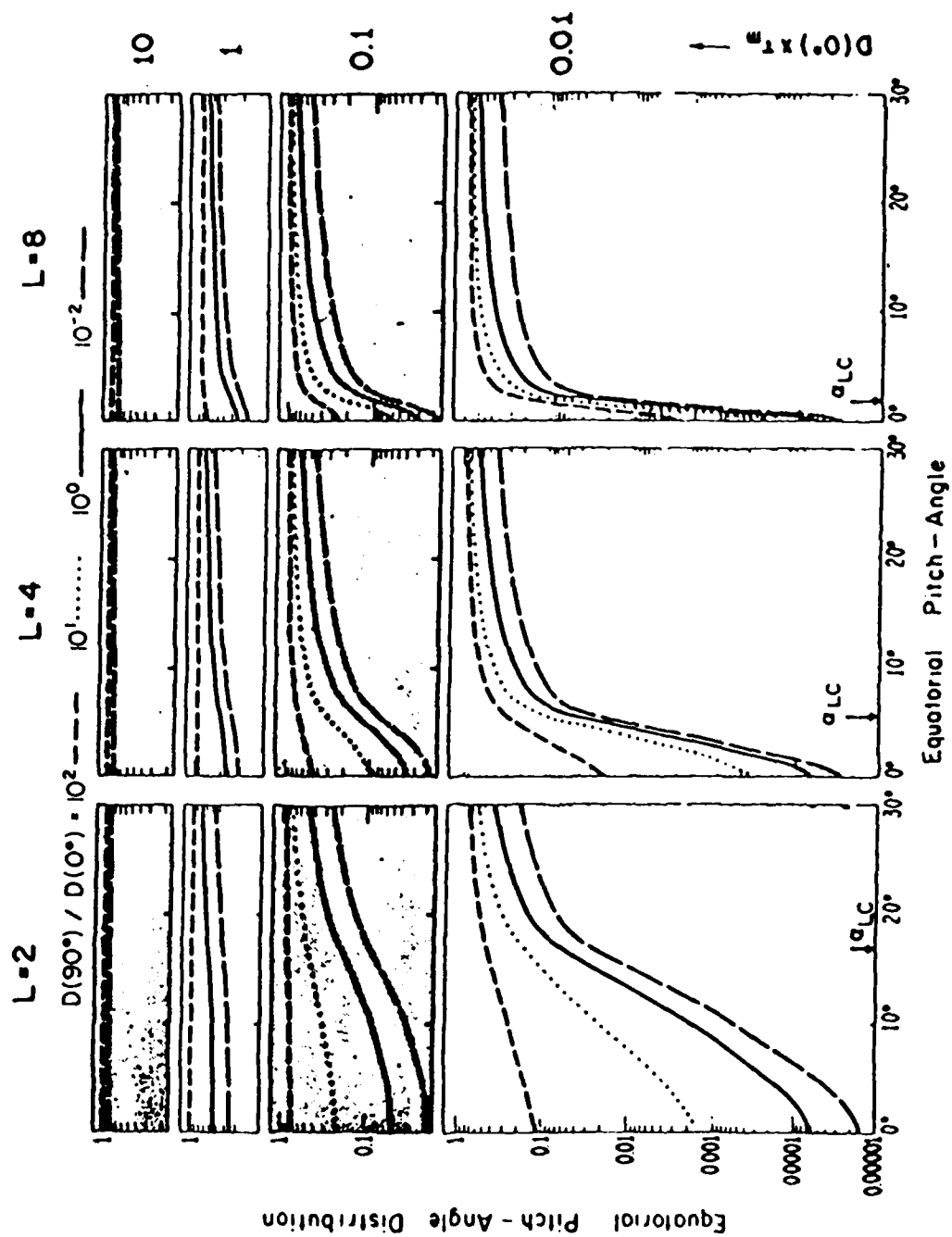
Figure 3-2

where $T_o = 4LRe/v$ (v is particle velocity) and $\eta$ is the probability of a particle being in the loss cone. $\eta$ is equal to the integral of the loss cone over the integral of the entire distribution.

$$\frac{\int_0^{\alpha_L} \sin\alpha_o \cos\alpha_o \, d\alpha_o}{\int_0^{\pi/2} \sin\alpha_o \cos\alpha_o \, d\alpha_o} = \sin^2\alpha_L \approx \eta \qquad (3\text{--}41)$$

Adding in the field line correction $2s(\alpha_o)$ for a dipole field

$$\eta = 2s(\alpha_o) \sin^2\alpha_L \qquad (3\text{-}42)$$

$$\tau_p = \tau_m = \frac{T_o}{\eta} \qquad (3\text{-}43)$$

Lyons [1973] went on to calculate numerical solutions for (3-37) to produce theoretical equatorial pitch angle distributions. He assumed no sources and a constant pitch angle distribution shape as the flux decayed. Values of $D(0°)$ and $D(90°)$ were chosen with $D(\alpha_o)$ allowed to vary linearly between $\alpha_o = 0°$ and $\alpha_o = 90°$. Note that the delineation between weak diffusion (3-10) and strong diffusion (3-12) is approximately $\dfrac{\alpha_L^2}{D_{\alpha\alpha}\,\tau_{1/4B}} = 1$;

where $D_{\alpha\alpha} = \dfrac{\alpha_L^2}{\tau_{1/4B}} \approx \tau_m^{-1}$. By normalizing $D(0°)$ to $\tau_m^{-1}$, solutions to (3-37) can be separated into diffusion regimes of very weak ($D(0°)\tau_m = 0.01$), weak (0.1), moderate (1), and strong (10). Plotted in Figure 3-2 are Lyon's solutions to (3-37) for $L = 2, 4,$ and 8.

## 3.5 ELECTROSTATIC CYCLOTRON HARMONIC WAVES AND DIFFUSION

The diffusion process presented thus far has been general and no scattering mechanism has been specified. Now we apply the Kennel et al. [1970] suggestion that ECH waves are responsible for pitch angle scattering in the near earth plasma sheet. Lyons [1974] quantified the Kennel et al. theory for $3/2\Omega$. ECH waves using quasi-linear diffusion. Kennel and Englemann [1966] presented a general quasi-linear diffusion

23

equation acted upon by a specific wave distribution. That equation for a space plasma in the presence of ECH waves is

$$\frac{\partial f}{\partial t} = \lim_{V \to \infty} \frac{i}{(3-2\pi)3} \, \Sigma_n \frac{q^2}{m^2} \int d3k \, \frac{|E_k|^2}{V \, |k|^2} \cdot \left( \frac{\pm n\Omega}{v_\perp} \frac{\partial}{\partial v_\perp} = k_{\parallel} \frac{\partial}{\partial v_{\parallel}} \right) \cdot$$
$$\frac{J_n{}^2 (k_\perp v_\perp/\Omega)}{vk - k_{\parallel} v_{\parallel} \pm (-n\Omega)} \cdot \left( \frac{\pm n\Omega}{v_\perp} \frac{\partial}{\partial v_\perp} = k_{\parallel} \frac{\partial}{\partial v_{\parallel}} \right) \tag{3-44}$$

where f is the spatially uniform zeroth-order distribution function in phase space, m is the plasma species rest mass, q is the charge, and $\pm$ refers to the sign of the charge. V is the plasma volume, $vk = \omega\kappa + \gamma_{\parallel}$ is the complex wave frequencies as a function of the wave number k, $E_k$ is the electric field at each k, $\Omega = (qB/mc)$ is the gyrofrequency, c is the speed of light, and Jn is a Bessel function of order n.

Equation (3-44) can be transformed from $f(v_\perp, v_{\parallel})$ to $f(v, \alpha)$

$$\frac{\partial f}{\partial t} = \nabla \cdot (D' \cdot \nabla f) = \frac{1}{v \sin \alpha \, \partial \alpha} \sin \alpha \left( D_{\alpha\alpha}' \frac{1}{v} \frac{\partial f}{\partial \alpha} + D_{\alpha v}' \frac{\partial f}{\partial v} \right)$$
$$+ \frac{1}{v^2} \frac{\partial}{\partial v} v^2 \left( D_{\alpha v}' \frac{1}{v} \frac{\partial f}{\partial \alpha} + D_{vv}' \frac{\partial f}{\partial v} \right) \tag{3-45}$$

where $D_{vv}$ is the diffusion coefficient in terms of speed. We are specifically concerned with the diffusion coefficient for electron interactions with electrostatic 3/2 $\Omega_-$ waves.

$$D_{\alpha\alpha} = \sum_{n=-\infty}^{\infty} D_{\alpha\alpha} n \tag{3-46}$$

The pitch angle diffusion coefficient is constrained by $\dfrac{|1.5 + n|}{.9} \leq \dfrac{v_{\parallel}}{v_{th\parallel}} < \dfrac{|1.5 + n|}{.1}$ and $D_{\alpha\alpha}{}^n = 0$ everywhere else.

Averaging $D_{\alpha\alpha}$ over a particle bounce period, as discussed previously in (3-32), Lyons [1974] was able to calculate numerical solutions for a normalized pitch angle coefficient,

$$\mathcal{D}_{\alpha\alpha} (\alpha_o, K/K_{th}) = <D_{\alpha\alpha}> \frac{K_{th}}{|E_w|_o{}^2} \tag{3-47}$$

where K is the particle energy, $K_{th}$ is the thermal energy, $|E_w|_o$ is the equatorial wave amplitude, and $<D_{\alpha\alpha}>$ is the bounce averaged diffusion coefficient. The results of

normalizing the diffusion coefficient to $K_{th}/|E_w|_o^2$ are shown in Figure 3-3. He assumed $K_{th\perp} = K_{th\parallel}$ and that K remain constant. The minimum $3/2\Omega_-$ wave amplitudes required to produce strong diffusion for various values of $K/K_{th}$ at L=7 are plotted in Figure 3-4.
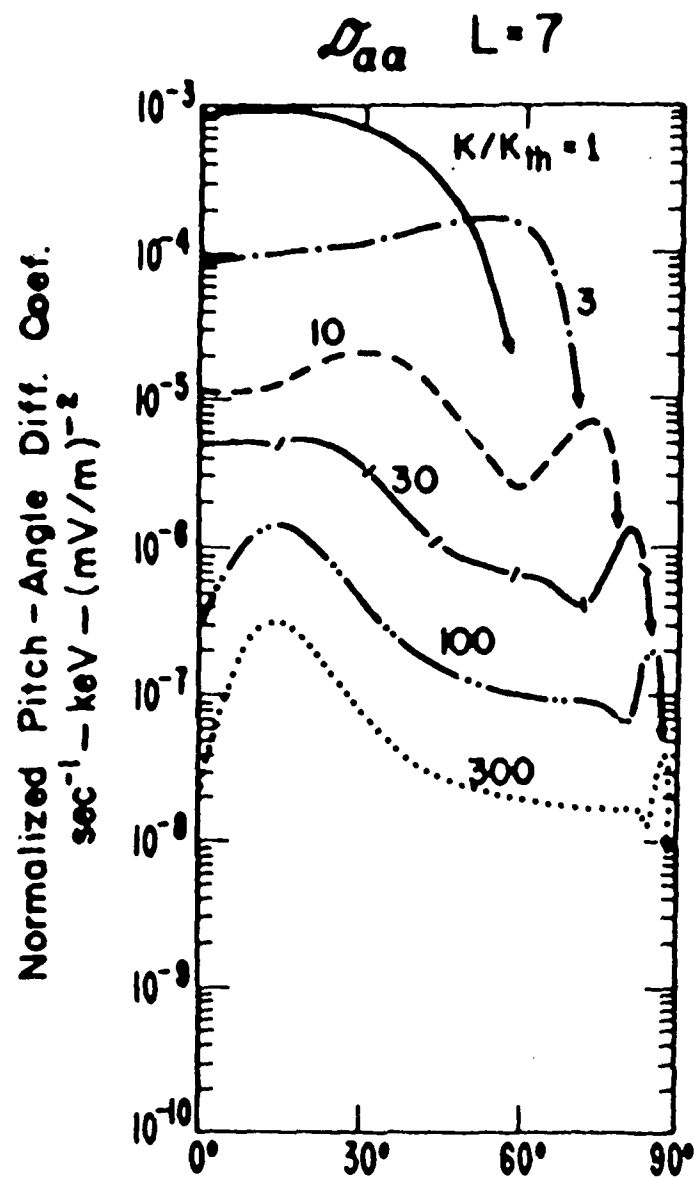
Figure 3-3. Normalized coefficients for diffusion in pitch angle $(D_{\alpha\alpha})$ are plotted as a function of equatorial pitch angle at $L = 7$ for representative values of the electron energy normalized to the thermal energy of the warm electrons. [From Lyons, 1974]
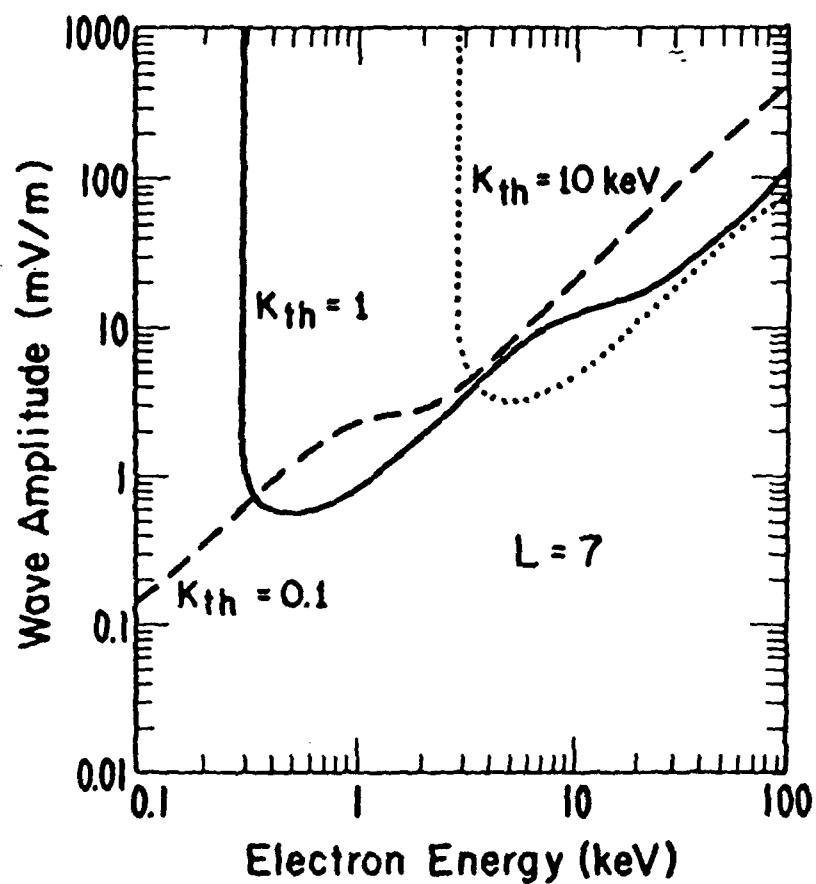
Figure 3-4. The minimum equatorial wave amplitude required for strong pitch angle diffusion at L = 7 is shown as a function of electron energy for thermal energies of 0.1, 1, and 10keV. [From Lyons, 1974]

# CHAPTER 4

# INSTRUMENTS

## 4.1 SCATHA (P78-2) SATELLITE

The Spacecraft Charging AT High Altitude (SCATHA) satellite, mission P78-2, is a joint United States Air Force/NASA vehicle. The primary objective of the satellite is to provide environmental and engineering information on the charging of spacecraft surfaces. A secondary objective is the collection of scientific data and is not necessarily related to spacecraft charging. A payload of nine experiments were provided by various members of the scientific community [Stevens and Vampola, 1978].

SCATHA was launched aboard a Delta rocket on 30 January 1979. The satellite reached final orbit on 2 February. P78-2 is in a near synchronous orbit generally within 8 degrees of the geographic equator. The orbit is elliptical with apogee at ~ 57000km (R ~ 8.9 Re) and perigee at ~ 33200km (R ~ 5.2 Re) geocentric. The orbit is inclined ~ 7.8 degrees from the earth's equatorial plane. SCATHA has an orbital period of ~ 23.6hrs. This period results in an eastward longitudal drift of ~ 5.3 degrees per day (see Fig. 4-1).

The P78-2 satellite body is cylindrical in shape with both a length and diameter of ~ 1.75m. The body is divided by a central (bellyband) portion which contains most of the experimental payload. Instruments sensitive to spacecraft influences are isolated on booms projecting from the bellyband. Shown mounted fore and aft of the bellyband in Figure 4-2 are solar cells. SCATHA design and construction is further detailed in Stevens and Vampola [1978] and Fennell [1982].

SCATHA spins about its axis at a rate of ~ 1rpm. During the period of interest (1979-82), the spin axis was in the plane of orbit directed towards dawn. (In 1986, the axis was lifted to its present position perpendicular to the orbital plane, in an effort to extend the life of the satellite.) The spin axis had to be maintained approximately normal to
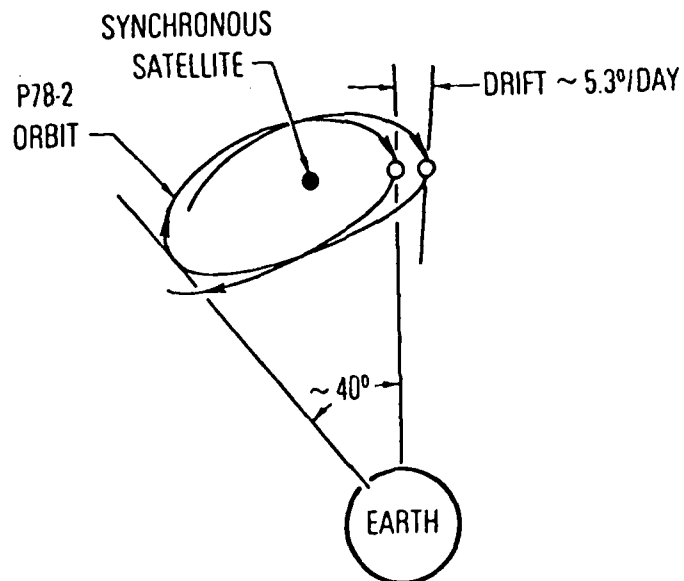
**MOTION OF P78-2 RELATIVE TO
A SYNCHRONOUS SATELLITE**



Figure 4-1. SCATHA orbital motion. The SCATHA satellite has a 23.6 hour orbital period resulting in a drift of ~5.3° per day. The subsatellite ground track is ~40° wide. [From Fennell, 1982]
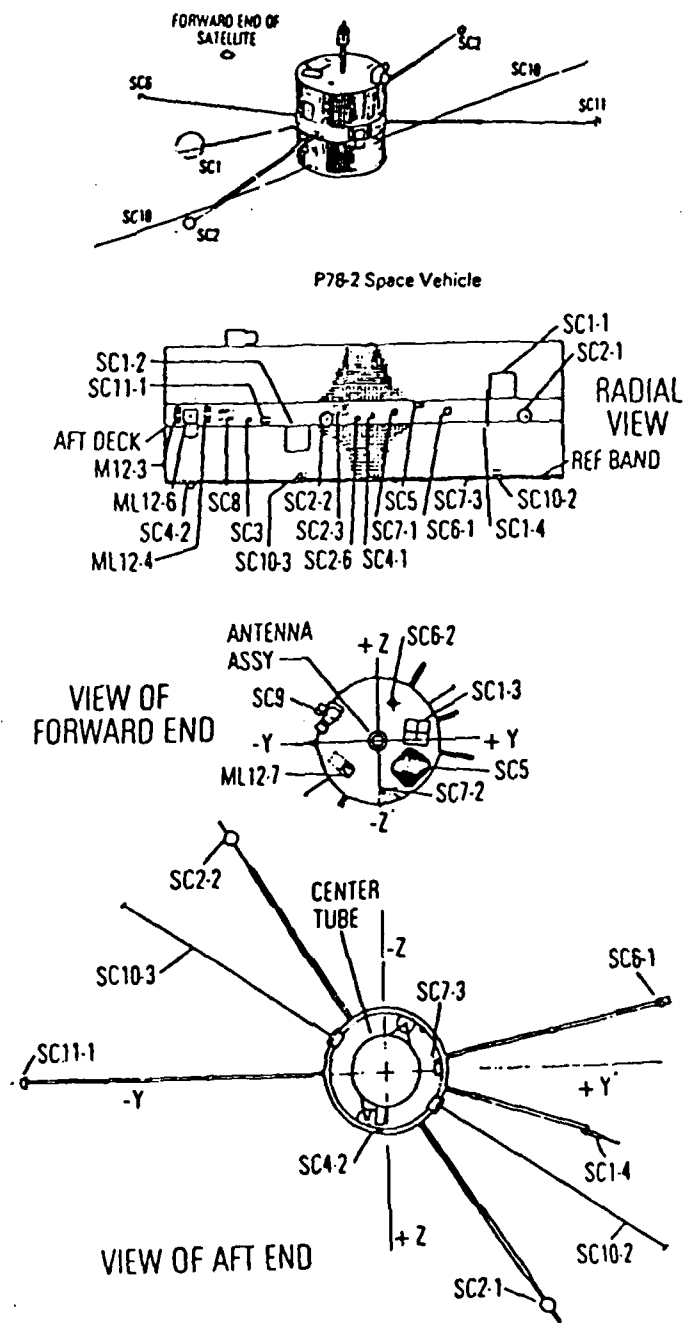
Figure 4-2. P78-2 SCATHA satellite and payload configurations. The SC2-3 is indicated on the radial view. [From Stevens and Vampola, 1978]

the satellite-sun line to maximize the efficiency of the solar cells. This orbital geometry required near weekly corrections to the satellite's orientation as the earth revolved about the sun. This geometry generally has the spin axis perpendicular to the magnetic field direction near local midnight.

## 4.2 SC2-3 ELECTROSTATIC ANALYZER

The data for this paper was collected by the SC2-3 Electrostatic Analyzer (ESA) aboard the SCATHA satellite. The SC2-3 ESA is one of a troika of Electrostatic Analyzers (i.e. SC2-1, SC2-2, and SC2-3). The primary objective of the ESA is to provide electron and ion distribution functions, between a few eV to ~20keV, at three positions in the spacecraft plasma sheath. The SC2-3 is located on the bellyband with a 360° field of view perpendicular to the spin axis.

The ESA consists of concentric cylindrical plates oppositely biased to deflect particles of the appropriate energy per charge. The plates are stepped through a cycle of biases. The center plate in Figure 4-3 is biased from ~ 0 to +1600V, while the two outside plates are simultaneously biased from ~ 0 to -1600V. The plates are serrated to eliminate particles that impact the sides and to reduce scattered light response. Particles succeeding in traveling the 127° curved path are detected in a Spiraltron channel electron multiplier.

Since electron data was used exclusively in the thesis, no further discussion of the ESA ion measurement capability is presented here. The electron geometric factor is ~1.7 x $10^{-4}$ cm$^2$ ster. The electron energy resolution is $\Delta E/E \sim 0.09$.

The electron spectrum is divided into 21 channels. The number of channels operating is programmable. Each channel collects data for 101.5msec after a ~23msec bias stabilization period. A complete 21 channel spectrum could be scanned in 3 seconds. The channels are subdivided into three programs as shown in Table 4-1. One program can be scanned in 1sec. The usual procedure during the period of interest was to only scan two

31
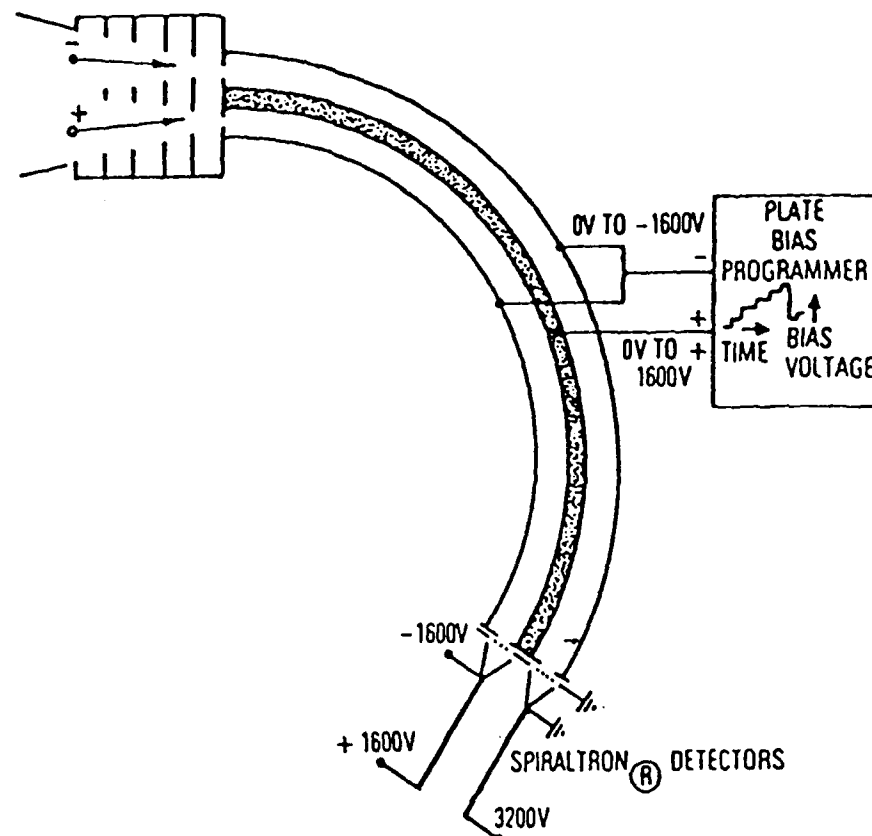
Figure 4-3. Cross-section of the Electrostatic Analyzer, SC2. [From Stevens and Vampola, 1978]

| SC2-3 ELECTROSTATIC ANALYZER | | |
|---|---|---|
| | STEP | ELECTRON ENERGY (eV/charge) |
| PROGRAM 1 | 0 | 187 |
| | 1 | 446 |
| | 2 | 1090 |
| | 3 | 2580 |
| | 4 | 4520 |
| | 5 | 10950 |
| | 6 | 19400 |
| | 7 | RETURN TO ZERO |
| PROGRAM 2 | 0 | BKG |
| | 1 | 87 |
| | 2 | 316 |
| | 3 | 815 |
| | 4 | 1940 |
| | 5 | 5900 |
| | 6 | 14400 |
| | 7 | RETURN TO ZERO |
| PROGRAM 3 | 0 | BKG |
| | 1 | 17 |
| | 2 | 40 |
| | 3 | 612 |
| | 4 | 1440 |
| | 5 | 3410 |
| | 6 | 8200 |
| | 7 | RETURN TO ZERO |

Table 4-1. SC2 Electrostatic Analyzer Electron Energies

programs at a time. This meant 14 channels were sampled 30 times per minute.

The ESA full width 10% maximum electron angular response was ~9° parallel and ~7° perpendicular to the spin axis. The full width half power points were ~5.5° parallel and ~5.8° perpendicular. The instrument response is represented as a product of a step function in the parallel and a Gaussian function in perpendicular directions, shown fitted to the data in Figure 4-4.

The response function becomes particularly significant when trying to observe electron pitch angle distribution features smaller than the angular response (e.g. the loss cone). Consider the geometry of Figure 4-5, where $\psi$ is the angular response, $\alpha_d$ is the detector pointing angle, B is the magnetic field, and $\xi$ is the phase angle. For pitch angles smaller than the angular response when the detector is field aligned (Fig. 4-5a), $\xi$ is completely contained within the angular response $\psi$. This is contrasted with the pitch angles where the detector is not field aligned (Fig. 4-5b). The result of integration over $\xi$ on small pitch angles is a large variation in the effective instrument response function as seen in Figure 4-6. At look angles $\alpha_d$ greater than $\psi$, the effective instrument response is constant. This instrument response function must be removed to gain a true measure of the pitch angle distribution. An algorithm to remove the response function is discussed in the Chapter 5.

Determination of field alignment is ascertained by a triaxial fluxgate magnetometer (SC11). The magnetometer is located at the end of a 4m boom (see Fig. 4-2). The axes of the sensor are accurately aligned with the vehicle. The SC11 samples four times a second with a resolution of $0.3\gamma$. The data was fit to the Olsen-Pfitzer [1974] magnetic field model.
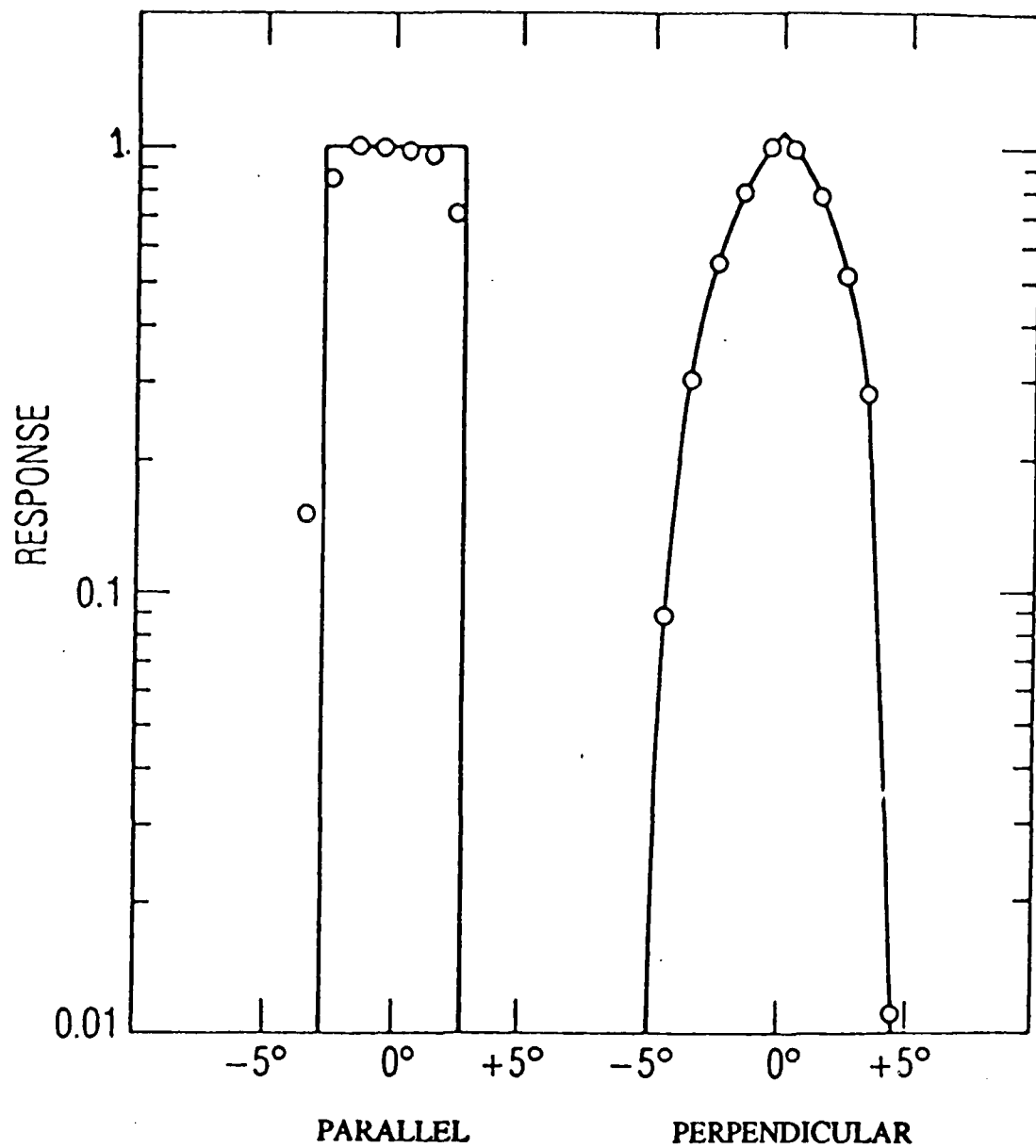
Figure 4-4. Representation of Electrostatic Analyzer as a product of a step function parallel to the spin plane of the spacecraft and a Gaussian function perpendicular to the spin plane. [From Roeder and Gorney, 1986]
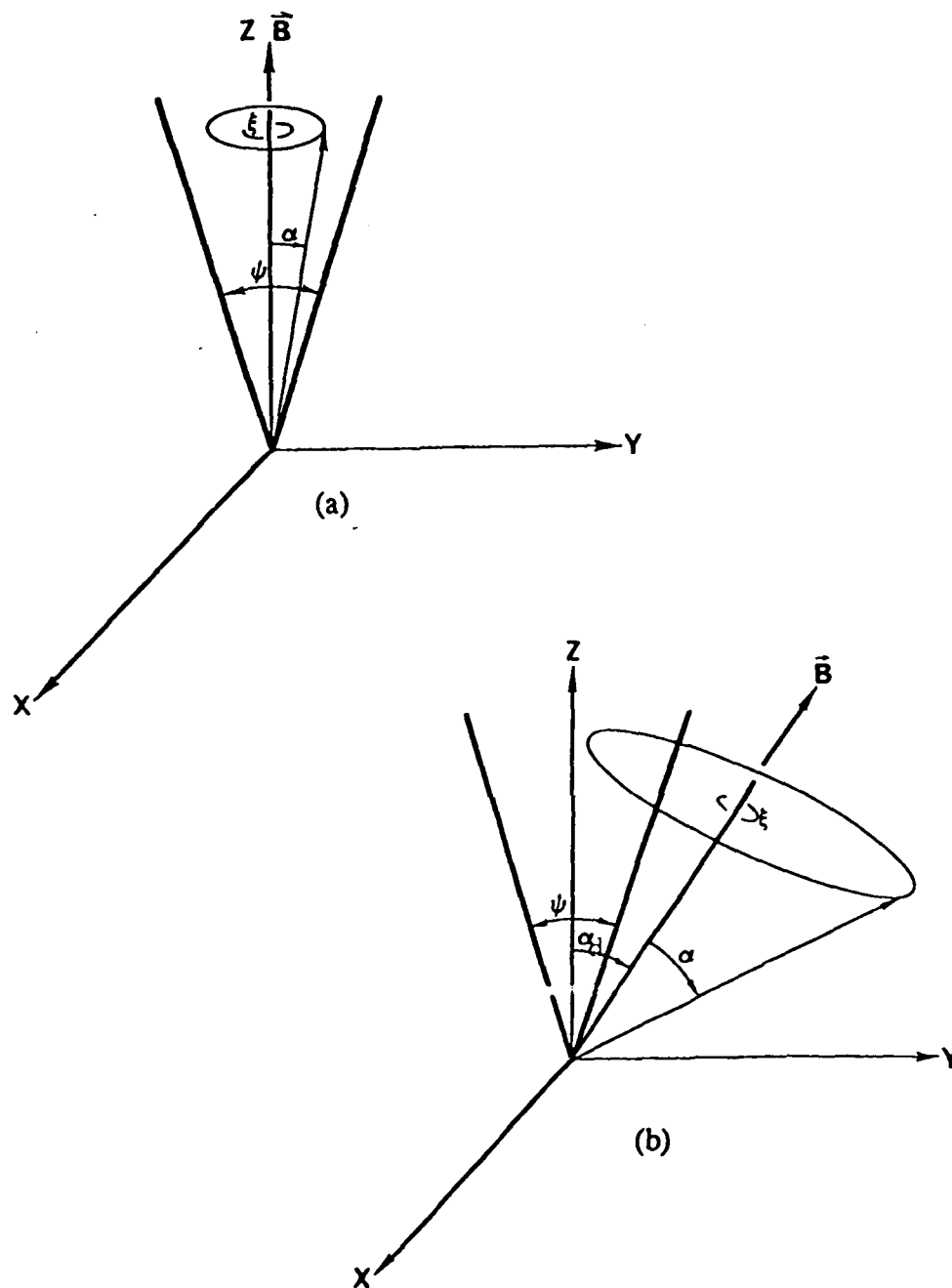
Figure 4-5. Geometry of the ESA pointing angle $\alpha_d$ and its effect on the pitch angle response function. (a) Pitch angle $\alpha$ is smaller than the angular response $\psi$ and will be completely contained within $\psi$ when the pointing angle is field aligned (i.e. $0°$). Integration of phase angles $\xi$ at $0°$ goes to 0, causing a significant variation in instrument response (see Fig. 4-6). (b) At large pointing angles, the variation in phase angle integration is smaller. [After Roeder and Gorney, 1986]

36
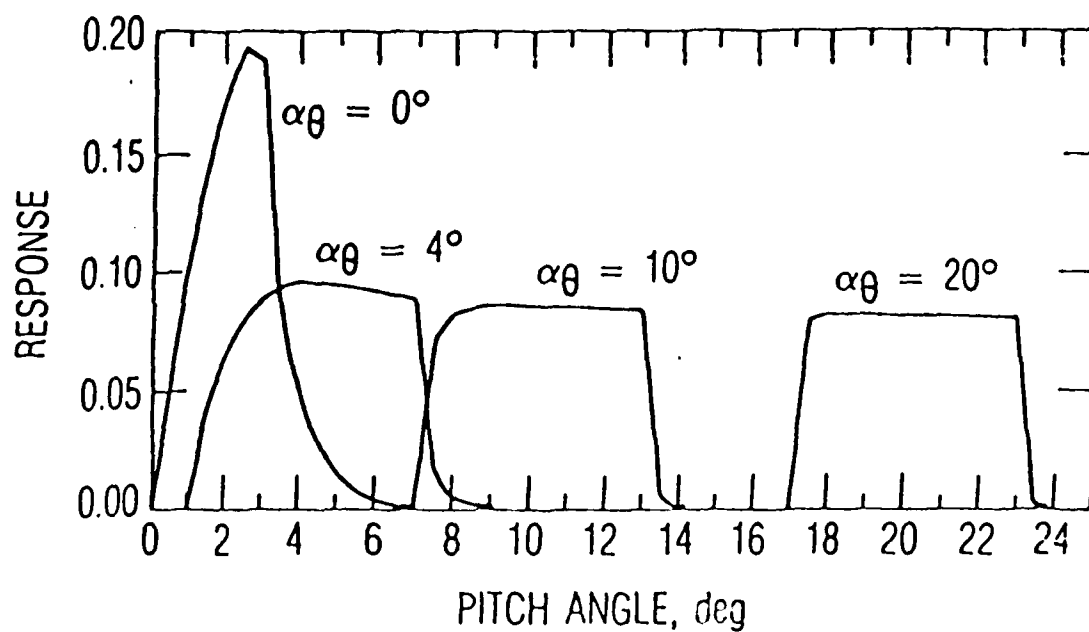
Figure 4-6. Pitch angle response function of the ESA for four detector pointing angles. Note the large variation in response at $\alpha_\theta = 0°$. [From Roeder and Gorney, 1987]

# CHAPTER 5

# DATA ANALYSIS AND OBSERVATIONS

## 5.1 ANISOTROPY

The first criteria for selection of data points was the observation of the loss cone. Observation of electrons in and near the loss cone is essential for any discussion of pitch angle diffusion. To ensure the ESA response included the loss cone (~2.5° at geostationary orbit) data points were selected only when the spin axis ($\vec{S}$) was perpendicular to the local magnetic vector $\vec{B}$ (90 ± 5°). This relationship between $\vec{S}$ and $\vec{B}$ was required to exists for a minimum of 15 minutes to allow adequate time for the collection of a statistically reliable sample. When the relationship remained for longer periods, a 15 minute window centered on the mid-point was chosen. A total of 617 nightside points were found between February 1979 and December 1982.

Seven electron channels were selected for examination; 0.187, 0.446, 1.09, 2.58, 4.52, 10.95, and 19.4keV. This energy range provides excellent coverage of the electrons primarily responsible for producing the diffuse aurora. These channels are also usually always available in the ESA data record.

ESA plots of parallel "$J_{\parallel}$" and perpendicular "$J_{\perp}$" electron counts for the period when $\vec{S}$ was nearly perpendicular to $\vec{B}$ were reviewed. The plots consist of an average plotted at each minute for $J_{\perp}(70\text{-}110°)$, $J_{\parallel}(0\text{-}30°)$, and $J_{\parallel}(150\text{-}180°)$. The mean includes the conjugate angles (181-360°). Figure 5-1 is a sample of ESA data where $J_{\perp}$ is plotted as a dot and $J_{\parallel}(0\text{-}30°, 150\text{-}180°)$ as larger symbols. Electron counts per second are plotted on a logarithmic scale which prevented simple 'eyeball' averaging for a 15 minute period. Instead, the value of the sample counts are median values for tightly grouped data points and selectively chosen values that best represent the period for widely scattered data. These

Figure 5-1. ESA data plots for 1.09, 1.94, 2.58, 4.52, and 5.9keV channels where $J_\perp$(70-110°) is plotted as a dot and $J_{\parallel}$(0-30°, 150-180°) as larger symbols. UT is universal time and MLT is magnetic local time. The magnetic field B is measured in gamma, L is in Re, and altitude (alt) is in Re. Note the 1.94keV electrons, (a)-(b) anisotropy ($J_\perp$>$J_{\parallel}$), (b)-(c) anisotropy ($J_\perp$<$J_{\parallel}$), and (c)-(d) approximate isotropy ($J_\perp$=$J_{\parallel}$).
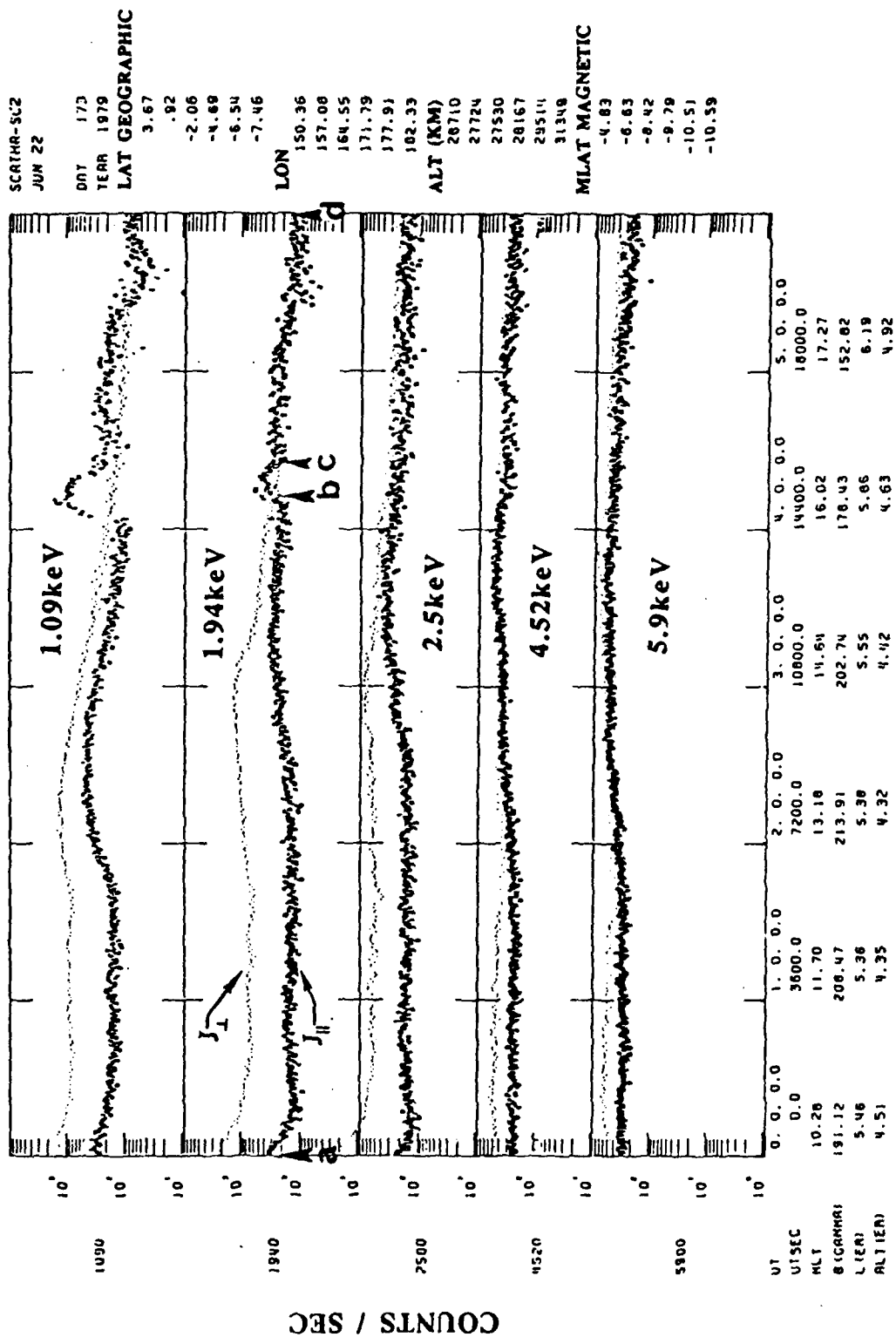
Figure 5-1

values were used to determine the ratio R of perpendicular to parallel electron counts in the pitch angle distribution.

$$R = J_\perp/J_\parallel \pm \sigma \tag{5-1}$$

The uncertainty $\sigma$ was determined assuming a Poisson distribution. Thus the total number of counts occurring within the 15 minute window must be calculated. This total count $J_{15}$ was computed for both the parallel and perpendicular direction.

$$J_{15_{\perp,\parallel}} = J_{i_{\perp,\parallel}}\ t_s\ t_o\ \rho \tag{5-2}$$

where $J_{i_{\perp,\parallel}}$ is the electron count per second selected to represent the 15 minute data sample, $t_s$ is the actual sampling time (i.e. 0.1sec), $t_o$ is the time of the observation (i.e. 15min), and $\rho$ is the average number of samples per minute. The number of samples is a function of the number of energy channels programmed to be collected and the number of degrees available for sampling in each direction (i.e. $J_\perp = \Delta 40°$ versus $J_\parallel = \Delta 30°$). The most common program, used during 72% of the observations, collected a count for a specific channel once every two seconds. Lesser used programs collected counts once every three seconds (26%) and once every one second (2%). In the case of a sample every two seconds, $J_\perp$ would be sampled an average of 6.7 times per minute (i.e. $6.7 = 1\text{sample}/2\text{sec} \times (40° \times 2)/6°\text{sec}^{-1}$). The uncertainty is taken for the ratio of total number of counts

$$\sigma = \frac{J_{15_\perp}}{J_{15_\parallel}} \left( 1 \pm \left( \frac{\sqrt{J_{15_\perp}}}{\sqrt{J_{15_\parallel}}} \right) \right) \tag{5-3}$$

The quoted $\sigma$ in this study is the average of the largest and smallest uncertainty.

$$\sigma = \frac{\dfrac{J_{15_\perp}}{J_{15_\parallel}} \left( \left( \dfrac{1 + \sqrt{J_{15_\perp}}}{1 - \sqrt{J_{15_\parallel}}} \right) + \left( \dfrac{1 - \sqrt{J_{15_\perp}}}{1 + \sqrt{J_{15_\parallel}}} \right) \right)}{2} \tag{5-4}$$

A trend/stability index was determined at each data point for every channel. The index noted trends towards increasing or decreasing electron counts as well as the stability of the trend for both $J_\perp$ and $J_\parallel$, individually. This index was required for further analysis when relatively stable periods would be required. The pitch angle anisotropy ($J_\perp > J_\parallel$), in

the distribution was also indexed in a similar manner.

The decision as to whether the observation was taken within the plasma sheet was subjective and is a source of uncertainty. This uncertainty increases in quiet time observations taken at the satellite's lowest altitudes (i.e. L<6), particularly in the pre-midnight bins. The points in these bins are not always within the mean plasma sheet inner edge extrapolated by Gussenhoven et al. [1981]. Rapid decreases in the electron counts were considered indications of the satellite moving out of the plasma sheet towards the plasmasphere. Extremely low or erratic count rates were eliminated.

Approximately 3400 pitch angle ratios for 7 energy channels at 493 different points in the plasma sheet were computed and considered valid. The spatial distribution of data points on the nightside is shown in Figure 5-2. The bulk of the distribution is in between 2200MLT and 0200MLT but there is adequate and nearly uniform coverage in the pre-midnight and post-midnight local times. The nightside coverage ranged in altitude from ~5.3L to ~8.8L.

Data points were binned into various ranges of local time, geocentric radius L, and geomagnetic activity levels. Local time bins included midnight (2200-0200MLT), pre-midnight (1800-2200MLT), and post-midnight (0200-0600MLT). L bins were divided into three ranges; $L < 6$, $6 \le L < 7$, $L \ge 7$. When combining the criteria for local time and L value nine bins are formed as shown in Figure 5-3.

The three hourly Kp index was selected for determination of geomagnetic activity binning because of its availability and relation to conjunctive boundaries of the diffuse aurora and the inner edge of the plasma sheet [Gussenhoven et al., 1981;1983]. Observations occurring during periods of $Kp \le 3$ were classified as quiet and those with $Kp > 3$ as active. Since the near earth plasma sheet may not return to pre-substorm electron densities for several hours after an injection [Roberts, 1969;Hoffman and Burch, 1973], these definitions were expanded. To account for possibly elevated post-injection electron
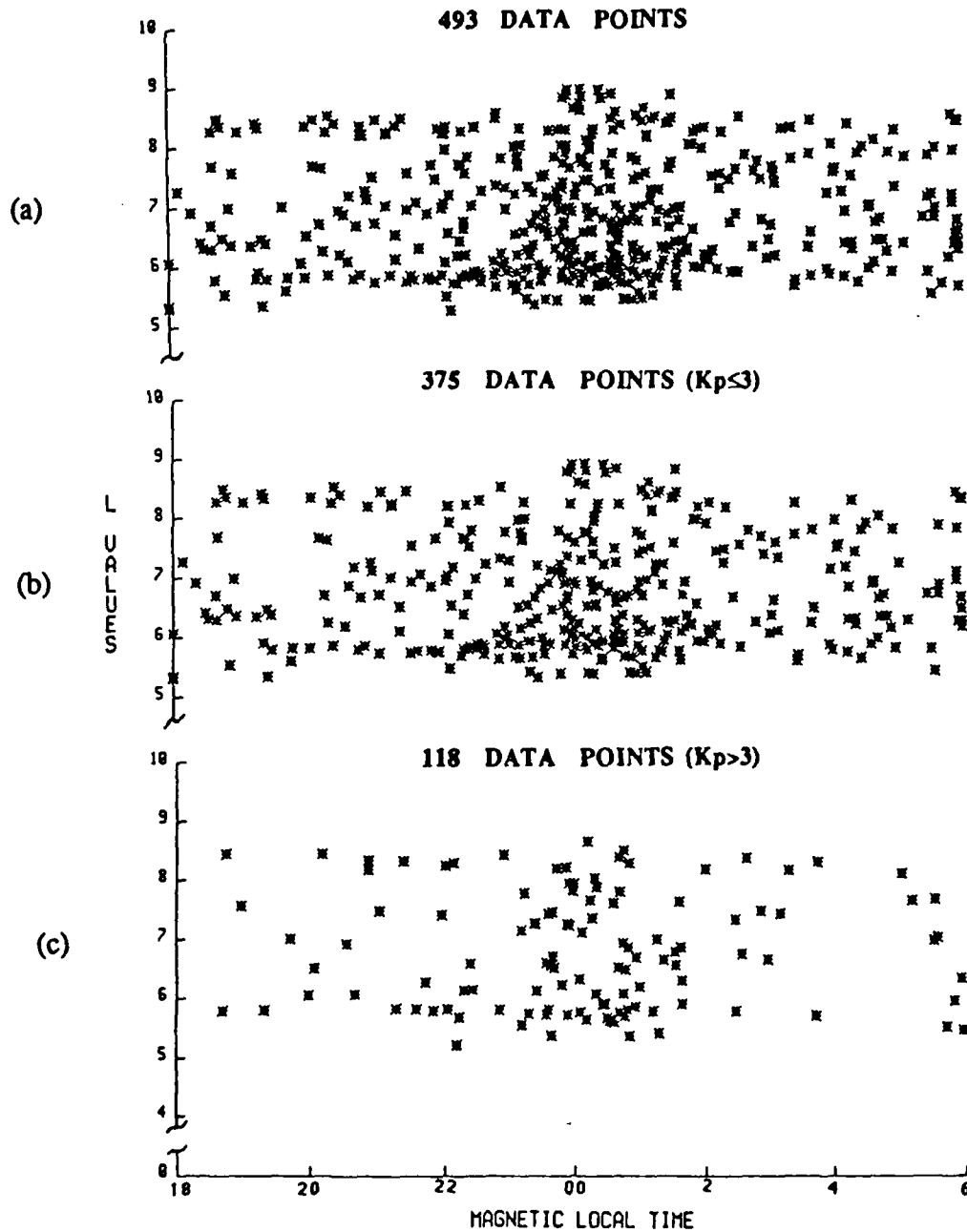
Figure 5-2. Spatial distribution of data points. (a) Seven energy channels at 493 different points in the plasma sheet were sampled. Observations occurring during periods of Kp ≤ 3 were classified as quiet (b) and those with Kp > 3 as active (c).
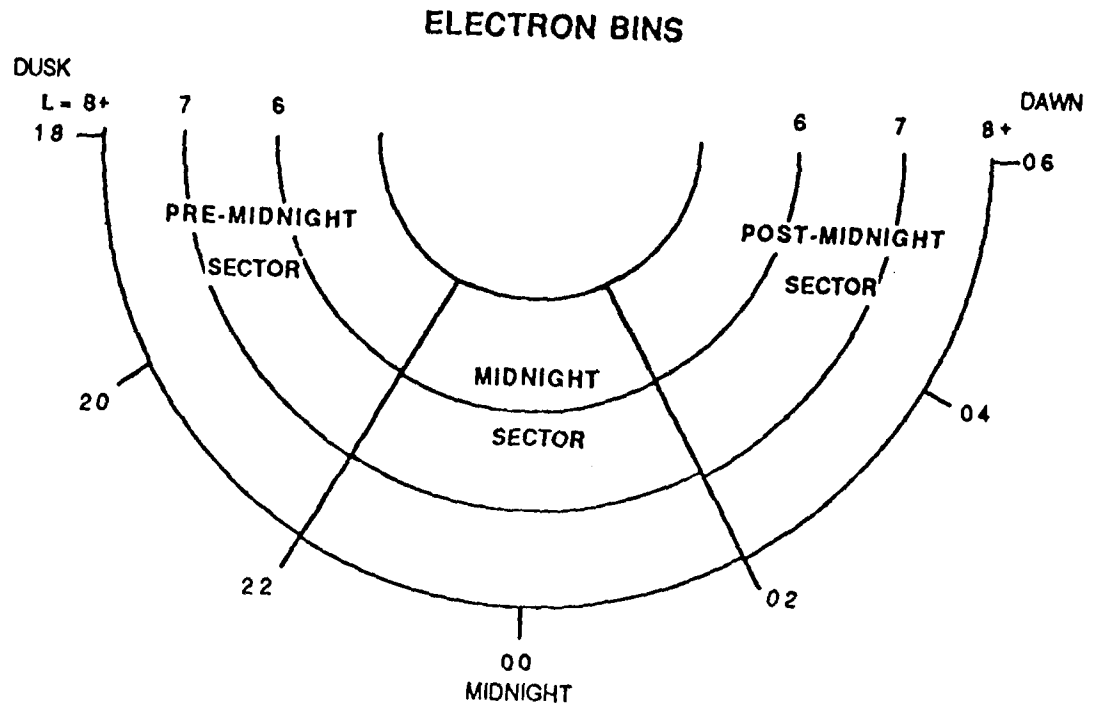
43

**ELECTRON BINS**



Figure 5-3. Data bins. Magnetic local time (MLT) and L value bins. Three MLT sectors are also indicated.

levels, quiet time observations occurring within the first two hours of a 3-hour Kp period required further examination. In these cases if the current Kp index was quiet but the preceding Kp period was active, the observation was binned as active. This insured that any observation classified as quiet was taken at least two hours after a substorm injection. This biased the less frequently occurring active observations toward quiet levels since a data point may occur as much as five hours after an injection and still be classified as active.

Table 5-1 contains statistics for the bins in Figure 5-3 for all Kp values and Table 5-2 for Kp≤3. The mean bin pitch angle ratio $R_{BIN}$ is given as well as the average uncertainty $\sigma_{BIN}$. Mean bin ratios were calculated as

$$R_{BIN} = \frac{\Sigma R_i}{n} \pm \sigma_{BIN} \tag{5-5}$$

where n is the number of observations and the uncertainty is defined

$$\sigma_{BIN} = \frac{\Sigma \sigma_i}{n} \tag{5-6}$$

Isotropy is defined as the percentage of observed bin samples where R is within one standard deviation of R=1. This standard deviation is determined from the average $\sigma$ of the R=1 samples from that bin. In cases where there were no isotropic samples present, values of equal energy from adjacent bins were used. Of the 375 quiet time samples isotropy varies from 0 to 30% with an average of 8 ± 7.7%. The addition of 118 active time samples increased the highest percentage of isotropy to 33% and increased the overall average isotropy to 9 ± 8.1%.

The mean quiet and combined (quiet and active) pitch angle distributions are all anisotropic ($J_\perp > J_{\parallel}$). The average anisotropies are plotted in Figure 5-4 and show several general trends. The weakest anisotropies (more isotropic) are at the largest L values (i.e. L ≥ 7). The anisotropy change is greatest between the L>7 and 6≤ L <7 regions at all local times. Generally, the largest anisotropies are in the post-midnight sector. These cases of

TABLE 5-1   BIN AVERAGES: anisotropy ($R_{BIN}=J_\perp/J_{||}$), uncertainty ($\sigma_{BIN}$), and % isotropy
for combined quiet and active times

| LOCAL TIME | L VALUE | | ENERGY (keV): 0.187 | 0.446 | 1.09 | 2.58 | 4.52 | 10.95 | 19.4 |
|---|---|---|---|---|---|---|---|---|---|
| 1800 - 2200 | L<6 | $R_{BIN}$ = | 3.84 | 3.83 | 2.71 | 2.32 | 2.18 | 2.06 | 1.78 |
| | | $\sigma_{BIN}$ = | 0.17 | 0.16 | 0.14 | 0.11 | 0.12 | 0.11 | 0.10 |
| | | ISOTROPY (%) = | 10 | 13 | 7 | 30 | 3 | 27 | 17 |
| 2200 - 0200 | L<6 | $R_{BIN}$ = | 2.17 | 2.49 | 2.40 | 2.25 | 2.41 | 2.33 | 2.03 |
| | | $\sigma_{BIN}$ = | 0.07 | 0.08 | 0.07 | 0.06 | 0.06 | 0.10 | 0.10 |
| | | ISOTROPY (%) = | 17 | 6 | 3 | 4 | 4 | 1 | 6 |
| 0200 - 0600 | L<6 | $R_{BIN}$ = | 4.30 | 4.45 | 4.30 | 3.57 | 3.06 | 2.89 | 2.96 |
| | | $\sigma_{BIN}$ = | 0.14 | 0.13 | 0.12 | 0.11 | 0.10 | 0.10 | 0.12 |
| | | ISOTROPY (%) = | 3 | 6 | 0 | 0 | 3 | 0 | 3 |
| 1800 - 2200 | 6≤ L <7 | $R_{BIN}$ = | 5.68 | 5.40 | 3.39 | 2.28 | 3.19 | 2.46 | 1.86 |
| | | $\sigma_{BIN}$ = | 0.26 | 0.30 | 0.16 | 0.12 | 0.22 | 0.15 | 0.14 |
| | | ISOTROPY (%) = | 11 | 10 | 12 | 13 | 8 | 7 | 10 |
| 2200 - 0200 | 6≤ L <7 | $R_{BIN}$ = | 2.32 | 2.35 | 2.08 | 2.18 | 2.09 | 1.93 | 2.01 |
| | | $\sigma_{BIN}$ = | 0.10 | 0.09 | 0.08 | 0.09 | 0.09 | 0.09 | 0.12 |
| | | ISOTROPY (%) = | 14 | 10 | 6 | 4 | 2 | 4 | 11 |
| 0200 - 0600 | 6≤ L <7 | $R_{BIN}$ = | 4.35 | 4.85 | 3.80 | 3.07 | 2.77 | 2.81 | 3.30 |
| | | $\sigma_{BIN}$ = | 0.11 | 0.12 | 0.10 | 0.07 | 0.06 | 0.08 | 0.13 |
| | | ISOTROPY (%) = | 15 | 7 | 7 | 0 | 0 | 0 | 0 |
| 1800 - 2200 | L≥7 | $R_{BIN}$ = | 3.32 | 3.70 | 2.25 | 1.94 | 2.46 | 2.10 | 1.90 |
| | | $\sigma_{BIN}$ = | 0.13 | 0.14 | 0.10 | 0.10 | 0.13 | 0.13 | 0.12 |
| | | ISOTROPY (%) = | 13 | 8 | 33 | 5 | 5 | 0 | 8 |
| 2200 - 0200 | L≥7 | $R_{BIN}$ = | 1.58 | 1.65 | 1.55 | 1.69 | 1.95 | 1.68 | 1.91 |
| | | $\sigma_{BIN}$ = | 0.07 | 0.06 | 0.05 | 0.05 | 0.06 | 0.07 | 0.10 |
| | | ISOTROPY (%) = | 26 | 34 | 21 | 14 | 12 | 13 | 16 |
| 0200 - 0600 | L≥7 | $R_{BIN}$ = | 2.94 | 2.58 | 2.39 | 2.49 | 2.20 | 2.70 | 2.47 |
| | | $\sigma_{BIN}$ = | 0.10 | 0.07 | 0.05 | 0.06 | 0.05 | 0.10 | 0.12 |
| | | ISOTROPY (%) = | 17 | 6 | 11 | | 0 | 0 | 3 |

TABLE 5-2   BIN AVERAGES: anisotropy ($R_{BIN}=J_\perp/J_\parallel$), uncertainty ($\sigma_{BIN}$), and % isotropy for quiet time ($KP \leq 3$)

| LOCAL TIME | L VALUE | | ENERGY (keV): 0.187 | 0.446 | 1.09 | 2.58 | 4.52 | 10.95 | 19.4 |
|---|---|---|---|---|---|---|---|---|---|
| 1800 - 2200 | L<6 | $R_{BIN}$ = | 3.29 | 3.13 | 2.48 | 3.41 | 2.20 | 2.26 | 1.78 |
| | | $\sigma_{BIN}$ = | 0.15 | 0.15 | 0.14 | 0.12 | 0.13 | 0.12 | 0.11 |
| | | ISOTROPY (%) = | 13 | 17 | 4 | 30 | 4 | 0 | 13 |
| 2200 - 0200 | L<6 | $R_{BIN}$ = | 2.20 | 2.95 | 2.25 | 2.28 | 2.51 | 2.19 | 1.95 |
| | | $\sigma_{BIN}$ = | 0.07 | 0.08 | 0.07 | 0.07 | 0.09 | 0.10 | 0.11 |
| | | ISOTROPY (%) = | 16 | 7 | 2 | 3 | 3 | 2 | 9 |
| 0200 - 0600 | L<6 | $R_{BIN}$ = | 4.33 | 4.34 | 3.54 | 3.43 | 2.97 | 2.80 | 2.82 |
| | | $\sigma_{BIN}$ = | 0.14 | 0.13 | 0.11 | 0.12 | 0.11 | 0.11 | 0.13 |
| | | ISOTROPY (%) = | 3 | 10 | 0 | 0 | 4 | 0 | 3 |
| 1800 - 2200 | 6≤ L <7 | $R_{BIN}$ = | 6.07 | 5.60 | 3.80 | 2.14 | 3.40 | 2.27 | 1.88 |
| | | $\sigma_{BIN}$ = | 0.28 | 0.32 | 0.13 | 0.12 | 0.24 | 0.14 | 0.13 |
| | | ISOTROPY (%) = | 10 | 14 | 10 | 0 | 5 | 10 | 0 |
| 2200 - 0200 | 6≤ L <7 | $R_{BIN}$ = | 2.66 | 2.60 | 2.19 | 2.29 | 2.26 | 1.97 | 2.03 |
| | | $\sigma_{BIN}$ = | 0.11 | 0.11 | 0.09 | 0.10 | 0.11 | 0.10 | 0.13 |
| | | ISOTROPY (%) = | 9 | 9 | 5 | 3 | 1 | 4 | 5 |
| 0200 - 0600 | 6≤ L <7 | $R_{BIN}$ = | 4.62 | 5.51 | 4.12 | 3.11 | 2.93 | 2.84 | 3.20 |
| | | $\sigma_{BIN}$ = | 0.12 | 0.14 | 0.11 | 0.08 | 0.06 | 0.09 | 0.12 |
| | | ISOTROPY (%) = | 13 | 4 | 0 | 0 | 0 | 0 | 0 |
| 1800 - 2200 | L≥7 | $R_{BIN}$ = | 3.33 | 3.81 | 2.24 | 2.00 | 2.49 | 2.12 | 1.86 |
| | | $\sigma_{BIN}$ = | 0.12 | 0.15 | 0.10 | 0.11 | 0.14 | 0.13 | 0.12 |
| | | ISOTROPY (%) = | 10 | 25 | 30 | 5 | 5 | 0 | 9 |
| 2200 - 0200 | L≥7 | $R_{BIN}$ = | 1.81 | 1.84 | 1.69 | 1.82 | 2.13 | 1.77 | 2.05 |
| | | $\sigma_{BIN}$ = | 0.08 | 0.06 | 0.06 | 0.06 | 0.07 | 0.08 | 0.12 |
| | | ISOTROPY (%) = | 24 | 26 | 5 | 13 | 11 | 13 | 19 |
| 0200 - 0600 | L≥7 | $R_{BIN}$ = | 3.48 | 3.00 | 2.71 | 2.71 | 2.36 | 3.00 | 2.63 |
| | | $\sigma_{BIN}$ = | 0.12 | 0.08 | 0.06 | 0.07 | 0.06 | 0.12 | 0.12 |
| | | ISOTROPY (%) = | 15 | 7 | 11 | 4 | 0 | 0 | 4 |

Figure 5-4. Bin anisotropy. Plots of representative samples of the average electron ratios $(J_\perp/J_\parallel)$ for 19.4keV bins of combined (quiet and active) (a-g) and quiet (h-n) geomagnetic activity. All the ratios are anisotropic $(J_\perp > J_\parallel)$.
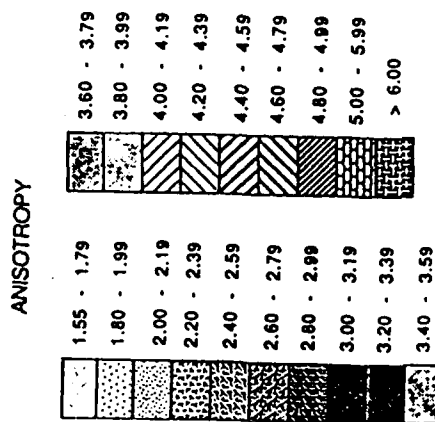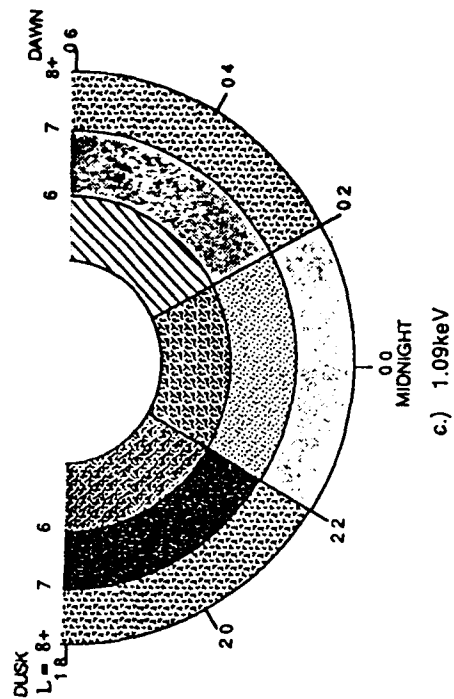
ANISOTROPY

| | | | |
|---|---|---|---|
| 1.55 - 1.79 | | 3.60 - 3.79 | |
| 1.80 - 1.99 | | 3.80 - 3.99 | |
| 2.00 - 2.19 | | 4.00 - 4.19 | |
| 2.20 - 2.39 | | 4.20 - 4.39 | |
| 2.40 - 2.59 | | 4.40 - 4.59 | |
| 2.60 - 2.79 | | 4.60 - 4.79 | |
| 2.80 - 2.99 | | 4.80 - 4.99 | |
| 3.00 - 3.19 | | 5.00 - 5.99 | |
| 3.20 - 3.39 | | > 6.00 | |
| 3.40 - 3.59 | | | |

a.) 0.187keV

b.) 0.442keV

c.) 1.09keV

Figure 5-4

49

e.) 4.52keV

g.) 19.4keV

d.) 2.58keV

f.) 10.9

50

h.) 0.187keV (Kp≤3)

i.) 0.446keV (Kp≤3)

j.) 1.09keV (Kp≤3)

k.) 2.58keV (Kp≤3)

51

l.) 4.52keV (Kp≤3)

m.) 10.95keV (Kp≤3)

n.) 19.4keV (Kp≤3)

52
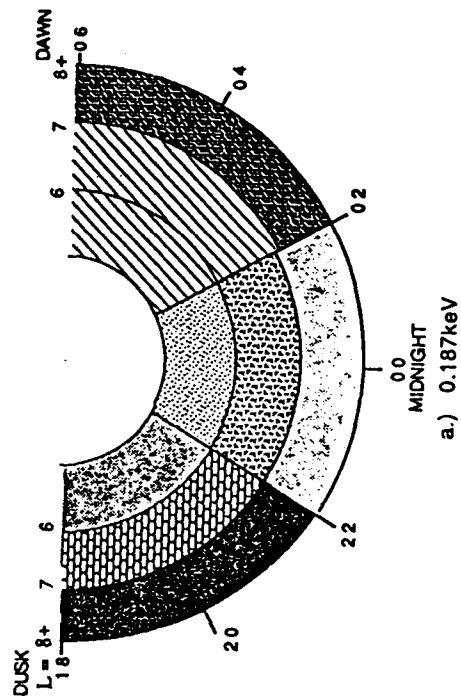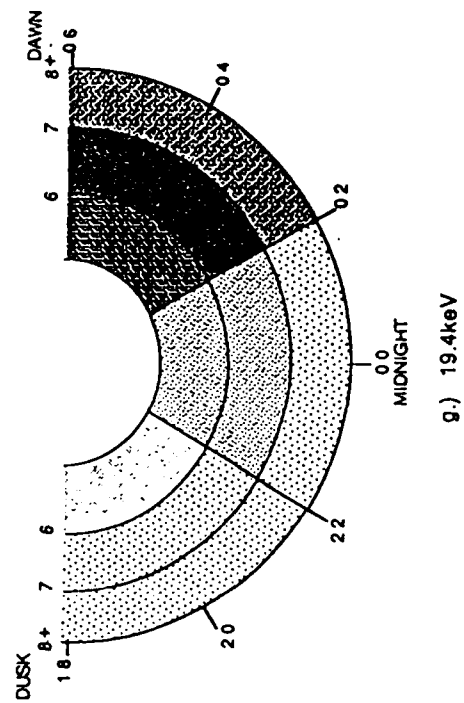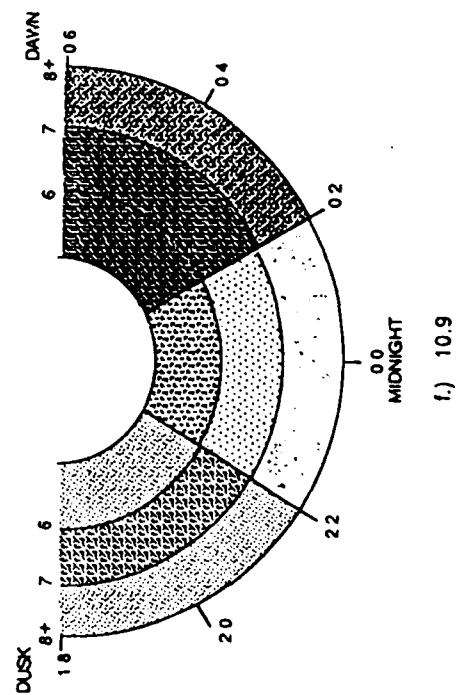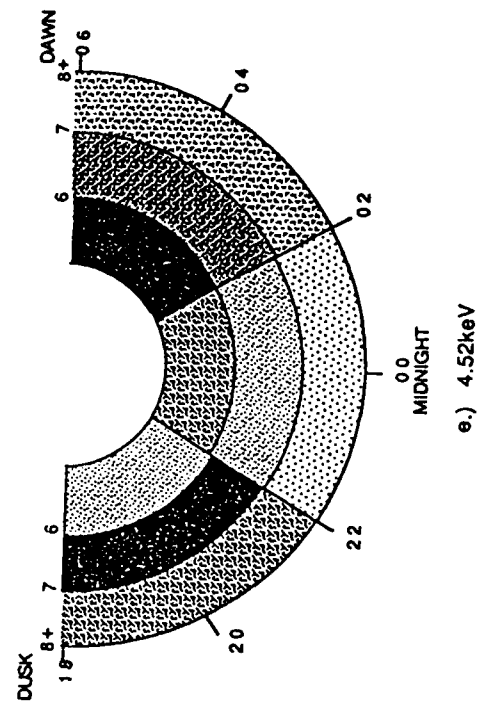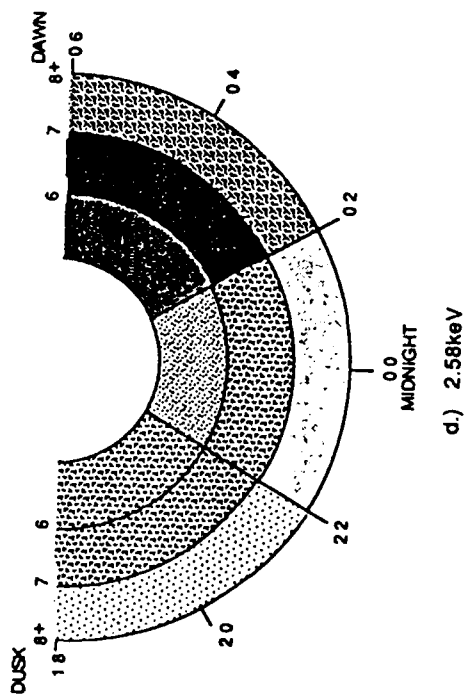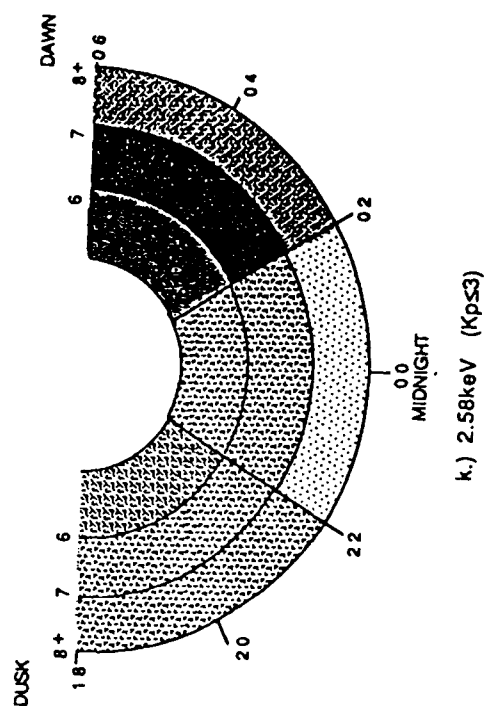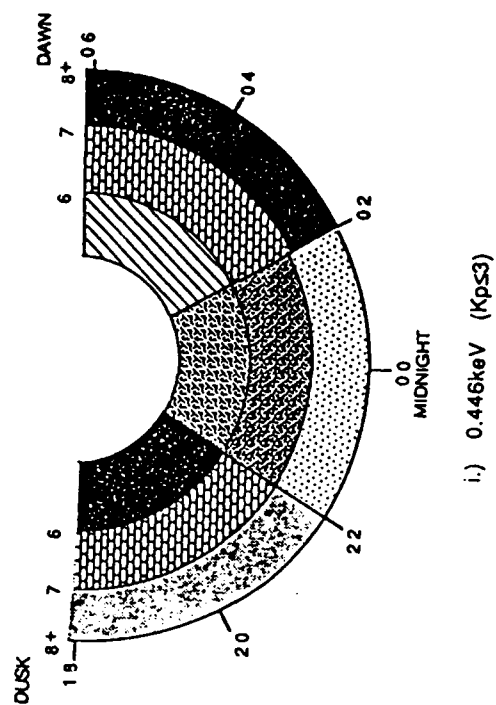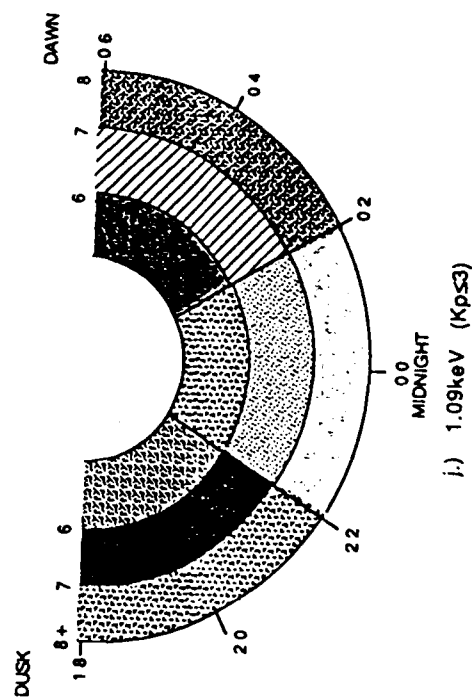
increasing anisotropy might be expected when an electron's trajectory, down the magnetotail and eastward around the earth, is considered. Electron trajectories computed by Ejiri [1978] show particle drift in the post-midnight sector slows down dramatically. It is hypothesized by Fairfield and Viñas [1983] that those particle distributions farthest along the drift trajectory have been acted upon by anisotropizing forces for a longer period of time. But this simple hypothesis fails in two other areas. First, the anisotropy increases as the particles move from distant magnetotail radially inward into the middle bins ($6 \leq L > 7$) then, in some cases, unexpectedly decreases as the particles continue earthward to $L < 6$. Anisotropy decreases at all energies in all the pre-midnight sector and in half of the energies in the post-midnight sector between $6 \leq L < 7$ and $L < 6$. Despite the decrease in anisotropy it is gre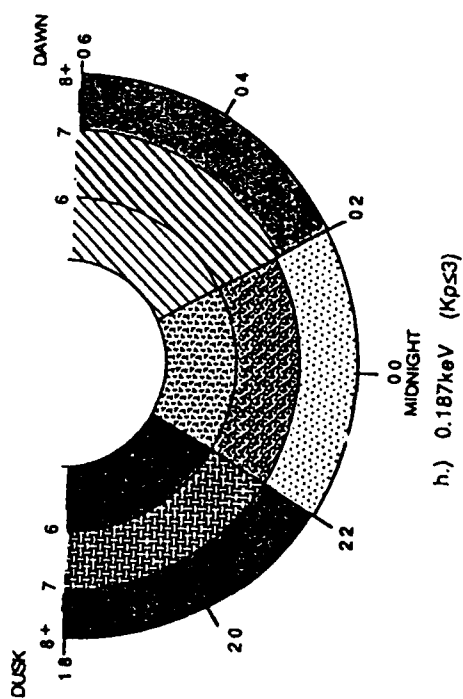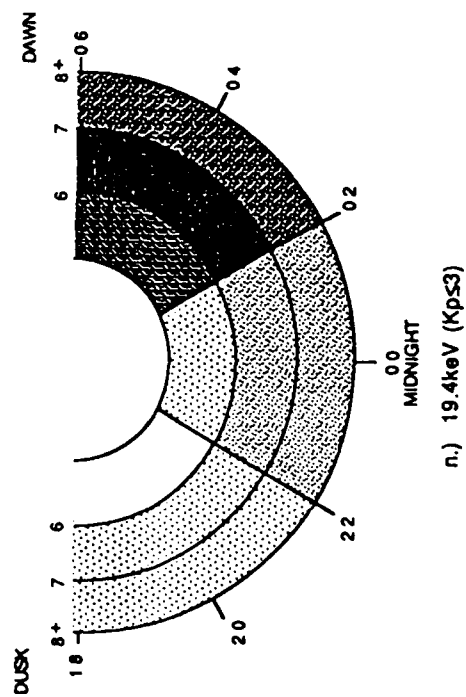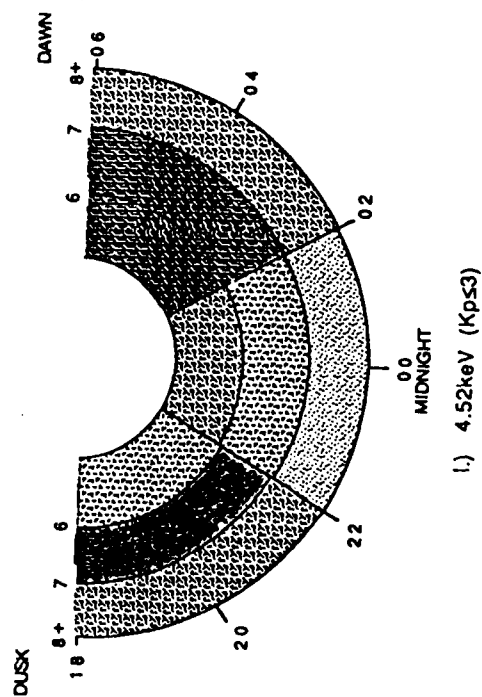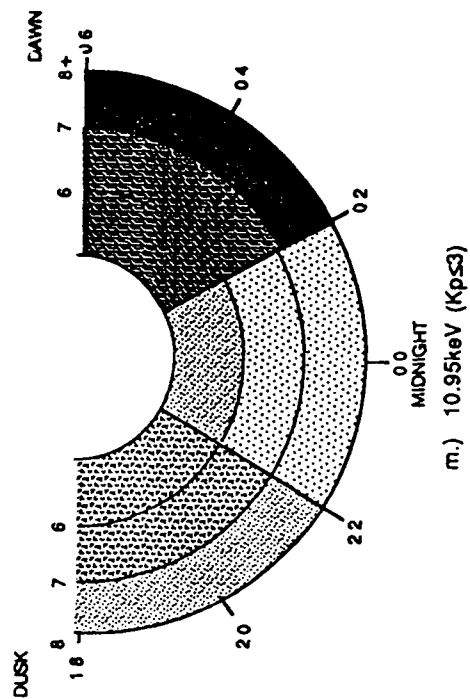ater in the innermost bins than in the $L > 7$ bins. Second, the anisotropy is greater in the pre-midnight bins than in the azimuthally downstream midnight bins. This latter contradiction may be evidence of plasmaspheric particles erroneously identified as being in the plasma sheet and adding to the anisotropy.

During active times isotropy is more prevalent. So as expected, $R_{BIN}$ at $Kp \leq 3$ is generally more anisotropic than $R_{BIN}$ at combined active and quiet Kp. This is particularly true at the lower energies. The higher energies (10.95 and 19.4keV) at quiet times show a mix of increasing, decreasing, and stable anisotropies relative to the same energies in the combined Kp bins.

The pre-midnight bins at $6 \leq L < 7$ for the two lowest energies (187 and 446eV) appear anomalously more anisotropic. This is due to a quarter of the pitch angle ratios in these bins possessing anisotropies greater than 7. These values appear to be valid but can not be immediately attributed to a specific phenomena. A follow-on investigation will be required to explain their appearance. When these high values are removed, the average anisotropy falls to levels more in line with those observed at higher energies.

An attempt to find a functional form to represent the various levels of anisotropies

53

was tried. Fits to $y\mathrm{Sin}^n\alpha$ and $x\mathrm{Sin}^m\alpha \pm y\mathrm{Sin}^n\alpha$ were initially promising but limited time to complete this thesis precluded a detailed study of such representations.

## 5.2 DIFFUSION

To examine the pitch angle distributions in the loss cone and determine the extent of diffusion, actual 15 minute data records had to be examined. The data records consists of the time in seconds, average pitch angle for that second and the counts per 0.1sec per channel. The process of retrieving specific 15 minute periods of data from the archived tapes was time consuming. If for some reason a data set was unavailable, incomplete, or otherwise unacceptable only a few could be replaced in a timely manner. Acting within this constraint the 19.4keV energy channel was initially selected for detailed analysis. This choice was an effort to avoid a local maximum in the distribution's loss cone (i.e. an anti-loss cone) created by secondary and backscattered electrons. This phenomenon is often present in energies up to a few keV [McIlwain, 1975]. Selection of representative sample distributions from each quiet time bin at 19.4keV were based on three criteria. First, the particle counts must have had a monotonic trend and stability. This eliminated the need to adjust the data for temporal changes during the 15 minute sampling period. Second, the trend/stability of the anisotropy also had to be monotonic. Finally, ratios $J_\perp/J_\parallel$ had to be within 10% of the mean anisotropy of their respective bin.

To obtain the true electron distribution, a deconvolution technique was applied to the data to remove the effects of the detector response function. This enabled features smaller than the detector's angular response width, such as the loss cone, to be discerned. The technique used was specifically developed for the SCATHA ESA data and was modeled after maximum-entropy schemes developed for image restoration and X-ray spectral deconvolution.

The statistical technique assumes the individual observations of electron flux are

related to the actual pitch angle distribution through a convolution function. The convolution function describes the response of the particle detector as a function of pitch angle. The deconvolved distribution can be obtained by maximizing the entropy of the electron distribution within the constraints of the convolution function and a Chi-squared error function. The algorithm is fully described by Roeder and Gorney [1986].

To facilitate the deconvolution program, data from the individual 0.1sec count periods between 91-180° were 'folded over' onto the observations between 0-90°. Then the counts C were averaged over 2° bins

$$C_{2^\circ} = \frac{\Sigma C_i}{n} \pm \sigma_{C_{2^\circ}} \qquad (5\text{-}7)$$

The uncertainty $\sigma_{C_{2^\circ}}$ was determined by

$$\sigma_{C_{2^\circ}} = \frac{\sqrt{\Sigma \sigma_i}}{n} \qquad (5\text{-}8)$$

The solid line in Figure 5-5 is an example of a reconstruction of the pitch angle distribution in 1° increments produced by the deconvolution algorithm. The counts are plotted as crossed error bars. The vertical error bar represents $\sigma_{C_{2^\circ}}$ and the horizontal bar is the instrument's full width response. The slight undulations in the plot are a manifestation of the 2° averaging and are not considered real. In every case recomputation of the pitch angle ratio from the reconstructed distribution produces a less anisotropic distribution than obtained from using only the $J_\perp/J_\parallel$ ratio. Anisotropies of 19.4keV electrons decreased on average $27 \pm 9\%$.

The extent of diffusion was determined by comparison of the deconvolved pitch angle distribution to the theoretical distribution computed by Lyons [1973] (see Fig. 3-2). Lyons' predicted equatorial pitch angle distributions were digitized for this purpose. The theoretical diffusion coefficients plots were then normalized to the intensity of the reconstructed distribution at 30° pitch angle. A plot of the theoretical diffusion coefficient which best fit the deconvolved pitch angle distribution was selected. Fits were determined

**4.520 keV Electron Pitch Angle Distribution**
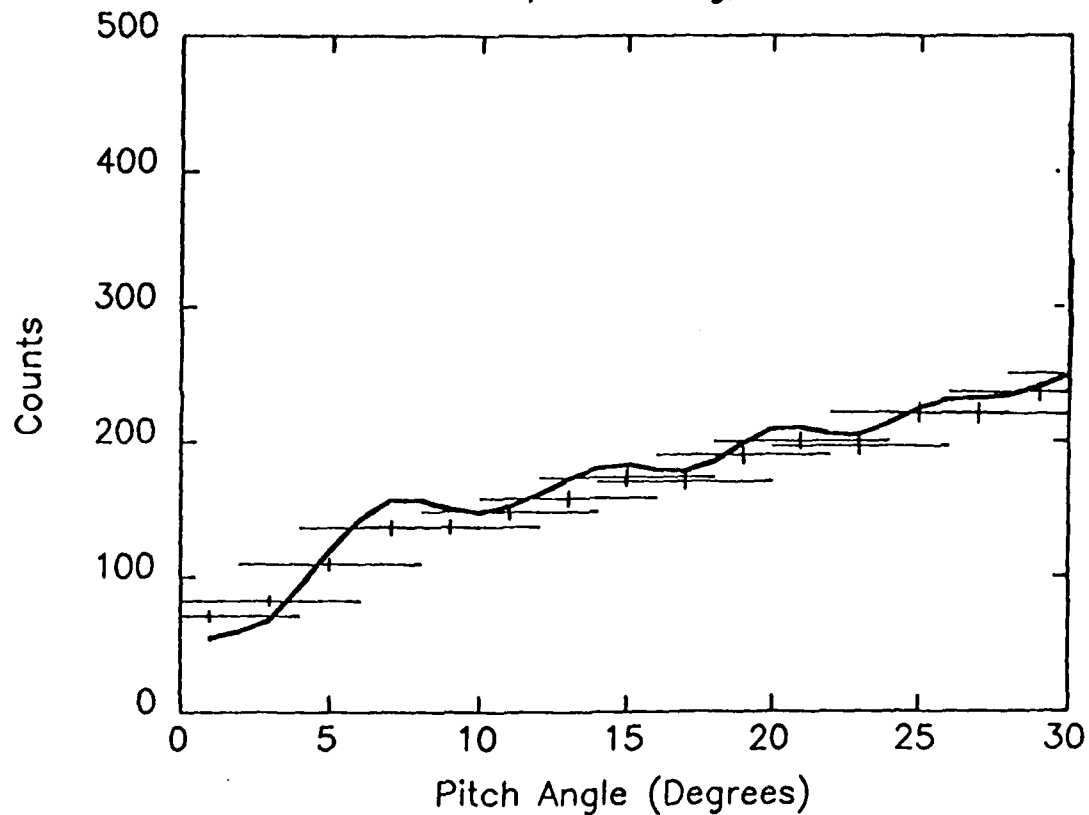**24 JUN 1979, 15min Avg, SG0=0.01**

Figure 5-5. Reconstructed pitch angle distribution. The solid line is the reconstruction of the pitch angle distribution in 1° increments produced by the deconvolution algorithm. The counts are plotted as crossed error bars where the vertical error bar represents $\sigma_{C_2}$, and the horizontal bar is the instrument's full width response. The uncertainty sg0 is 0.01.

Decovolution Pitch–Angle Distibution

(a) 4.52keV  Moderate diffusion
$R = 2.21$   $D(0°)\tau_m = 1$
$R_{DEC} = 1.46$   $D(90°)/D(0°) = 10^{-2}$

(b) 19.4keV  Moderate diffusion
$R = 1.78$   $D(0°)\tau_m = 1$
$R_{DEC} = 1.40$   $D(90°)/D(0°) = 10^{-2}$

(c) 19.4keV  Moderate diffusion
$R = 1.17$   $D(0°)\tau_m = 1$
$R_{DEC} = 0.95$   $D(90°)/D(0°) = 10^{-2}$

(d) 4.52keV  Weak diffusion
$R = 2.69$   $D(0°)\tau_m = 0.1$
$R_{DEC} = 1.85$   $D(90°)/D(0°) = 10$

(e) 1.09keV  Weak diffusion
$R = 2.21$   $D(0°)\tau_m = 0.1$
$R_{DEC} = 1.77$   $D(90°)/D(0°) = 10^2$

(f) 19.4keV  Weak diffusion
$R = 2.70$   $D(0°)\tau_m = 0.1$
$R_{DEC} = 1.75$   $D(90°)/D(0°) = 10^2$

Average Pitch–Angle

Figure 5-6. Fits of observed electron distributions to theoretically diffused distributions. The heavy solid line is the deconvolved distribution and the dashed line is the best fit predicted angular distribution which would result from moderate (a-c) to weak diffusion (d-f) from Lyons [1973]. Given for each fit are the observed anisotropy R, the deconvolved anisotropy $R_{DEC}$, and the diffusion coefficients $D(0°)\ \tau_m$ and $D(90°)/D(0°)$.

57

by eye. Figure 5-6 is an illustration of sample fits used to derived the relative diffusion for various energy levels. The heavy solid line is the deconvolved distribution and the dashed line is the best fit predicted angular distribution which would result from moderate to weak diffusion. Cases 5-6a-c represent fits corresponding to moderate diffusion while cases 5-6d-f are consistent with weak diffusion. The original and deconvolved anisotropies are also noted in Figure 5-6.

Figure 5-7 illustrates the various estimates of diffusion rates obtained for 19.4keV electrons. All the 19.4keV mean bin ratios in Figure 5-7a equated to moderate diffusion, save one. The exception was the most anisotropic average ratio (R=3.20) located in the post-midnight sector at $6 \leq L < 7$. This ratio was consistent with weak diffusion. Observations representing the mean anisotropy in MLT (integrated over all L) and L (integrated over all MLT) values are shown Figure 5-7b and 5-7c, respectively. Figure 5-7d is an example of a nearly isotropic distribution. An opposite case, strong anisotropy, is shown in 5-7e for the same bin. The nearly isotropic case corresponds to moderate diffusion while the very anisotropic case corresponds to weak diffusion. As expected stronger diffusion would be required to isotropize the distribution in 5-7d.

A second data set for 4.52keV particles was subsequently examined. An energy level below 10keV was suggested as being more representative of the diffuse aurora and closer aligned to the work of Lyons [1974] [Lyons, personal communications, 1990]. To get convergence a slight change had to be made to the deconvolution algorithm. The uncertainty used in the deconvolution algorithm is

$$\sigma_{decon} = \sigma_{A_2\circ} + fx \, sg0 \tag{5-9}$$

where fx is the electron count and sg0 is a constant. The sg0 factor widens the uncertainty to achieve convergences in cases with large temporal variations. The default value of sg0 is 0.01. The uncertainty sg0 was raised to 0.05 for several of the 4.52keV electron angular distributions. The results were six viable deconvolved pitch angle distributions with weak

58

Figure 5-7. Theoretical diffusion of quiet time 19.4keV electron distributions. (a) Estimated diffusion of pitch angle distributions representative of the mean bin anisotropy. Observations of distributions representing the mean anisotropy in MLT (b) and L value (c). Estimated moderate diffusion is present in (d) for a nearly isotropic distribution (R=1.17) while estimated weak diffusion is found in (e) for the very anisotropic (R=270).
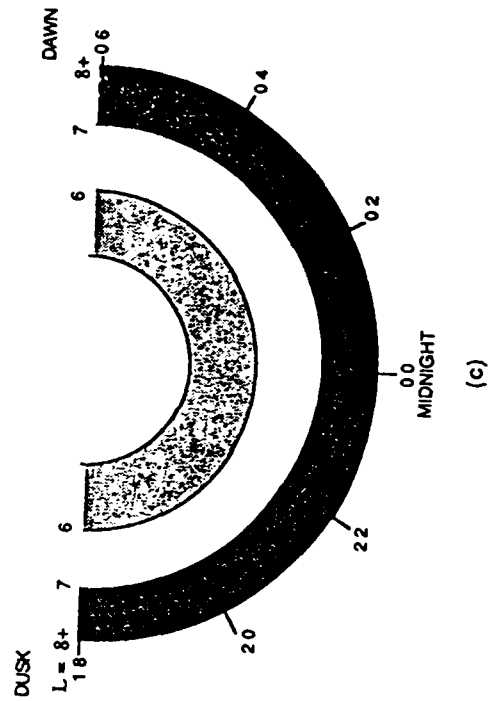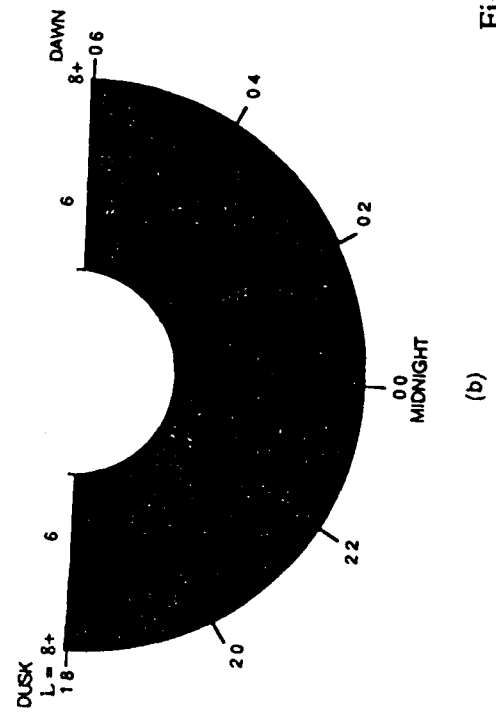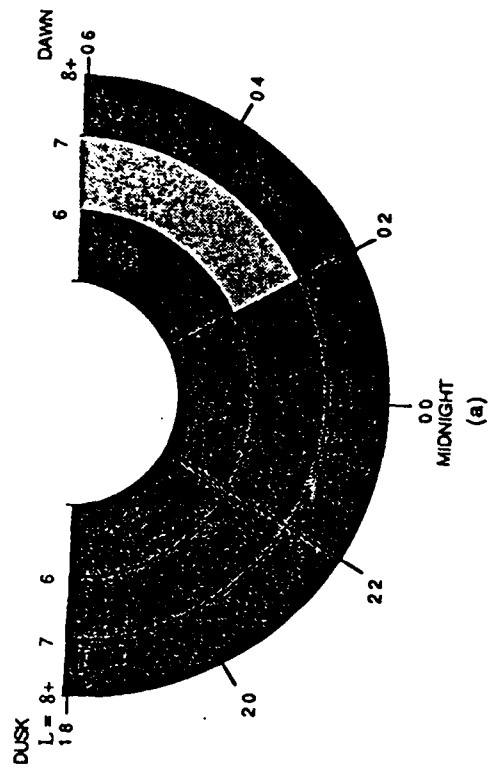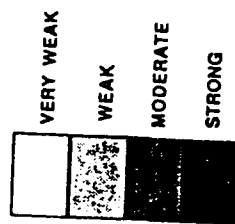
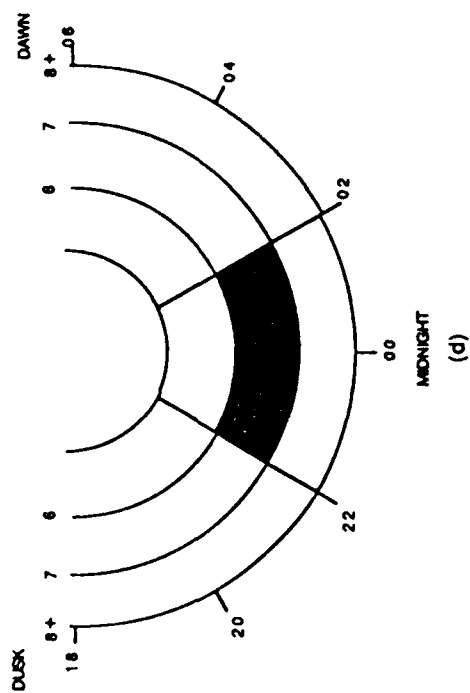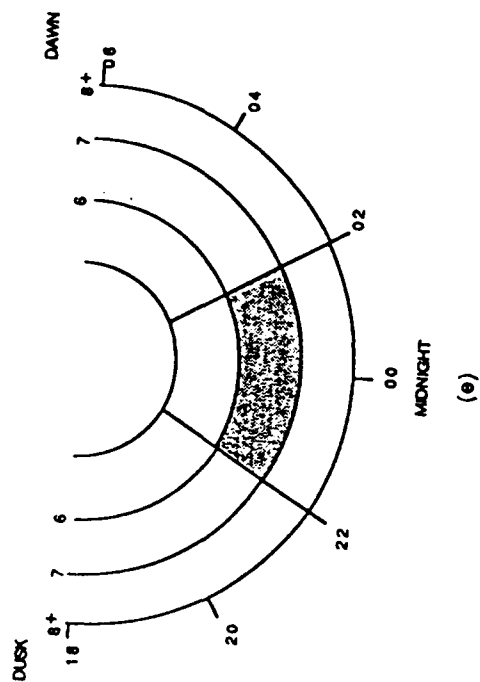THEORETICAL DIFFUSION OF 19.4KEV ELECTRONS



Figure 5-7

(d)



(e)

61

to moderate diffusion (see Fig. 5-8). The reconstructed anisotropies decreased an average of $25 \pm 9\%$ from those obtained using only the $J_\perp/J_\parallel$ ratios.

A final estimate of the diffusion rate was obtained using 1.09keV electron data. This set of data did not meet the same strict requirements of the previous ones. It was a target of opportunity, having been extracted from the same data set used for the 4.52keV electron study. The anisotropy of these samples ranged from within 1 to 54% of the mean anisotropy of their respective bins (see Fig. 5-9). The presence of an anti-loss cone caused the rejection of several 1.09keV angular distributions. The deconvolved distributions had an average decrease in anisotropy of $21 \pm 10\%$ relative to that obtained from the $J_\perp/J_\parallel$ ratios.

An inherent uncertainty in the manner in which the raw counts were tabulated is present in the results shown in Figures 5-7,8,9. The pitch angle assigned to each second of raw data represents the center of a $6°$ angular bin (the angular distance covered by the sensor in 1sec.). The sequential order in which the energy channels are observed plus other instrumental factors determines the amount of pitch angle error. The greatest pitch angle errors would be for the first and last channel sampled within that second. This meant there was a $2.8°$ error for the raw 19.4keV data points, ~$0.6°$ error for the 4.52keV data and ~$1.1°$ error for the 1.09keV data. This systematic error does not appear to make a significant difference in the results. The estimated diffusion rates for 19.4keV electrons is of the same magnitude or only slightly higher than that estimated for the 1.09 or 4.52keV electrons, despite the ~$1°$ larger systematic pitch angle offset for the 19.4keV data.

## 5.3 ECH WAVE AMPLITUDE

The ECH wave amplitude required to create the reconstructed distribution was determined by adapting Lyons [1974] normalized pitch angle diffusion coefficient equation (3-47) and solving for the wave amplitude
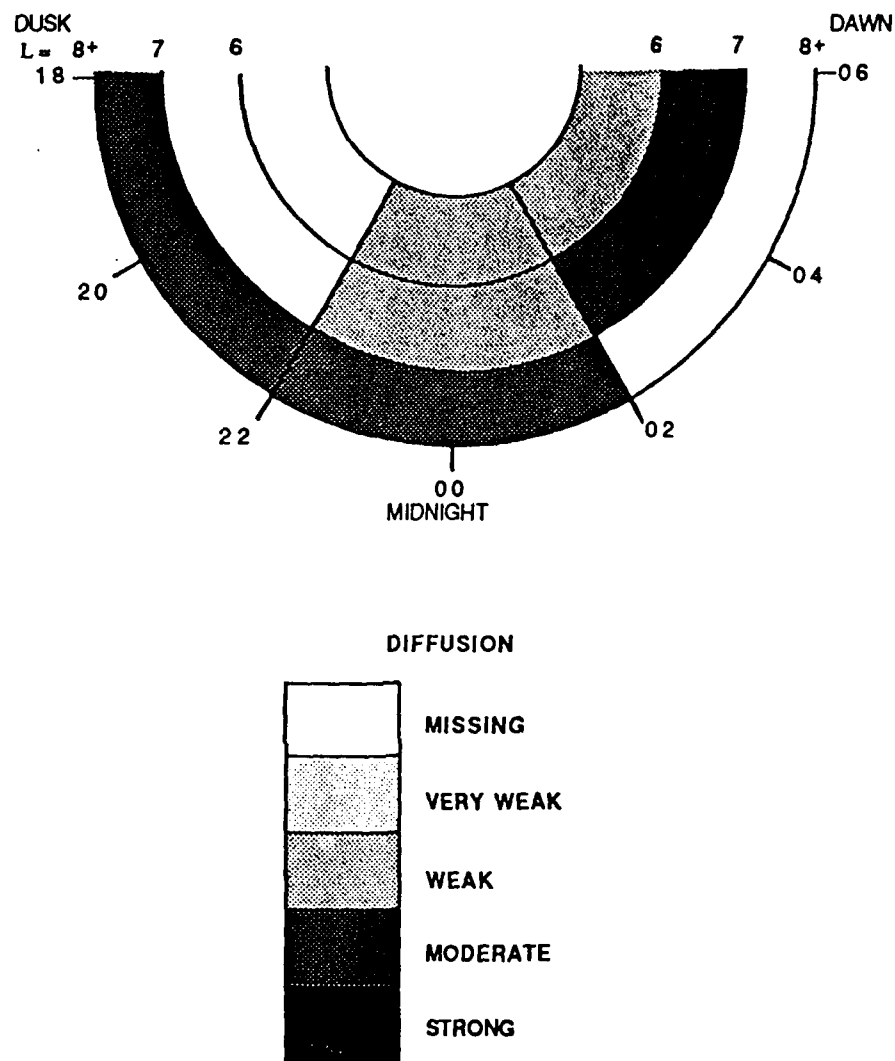
# THEORETICAL DIFFUSION OF 4.52KEV ELECTRONS



Figure 5-8. Estimated diffusion of 4.52keV electron distributions representing the mean anisotropy of the quiet time bins.

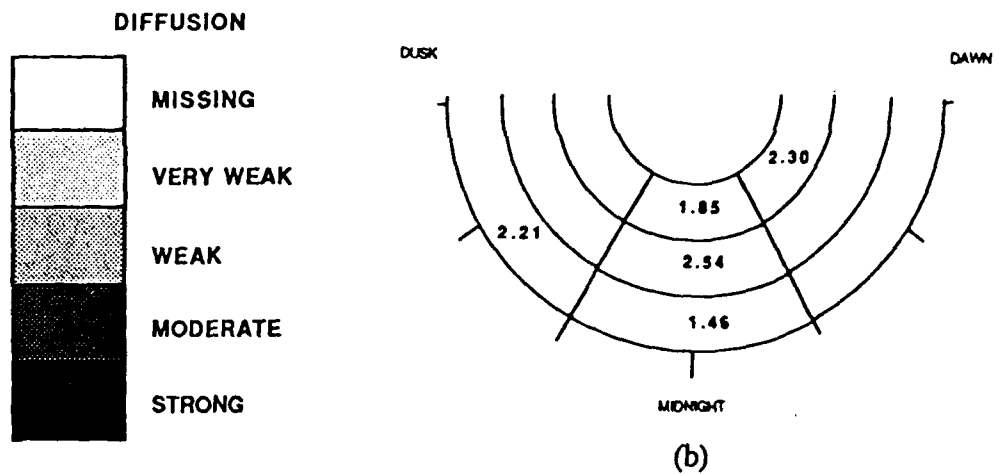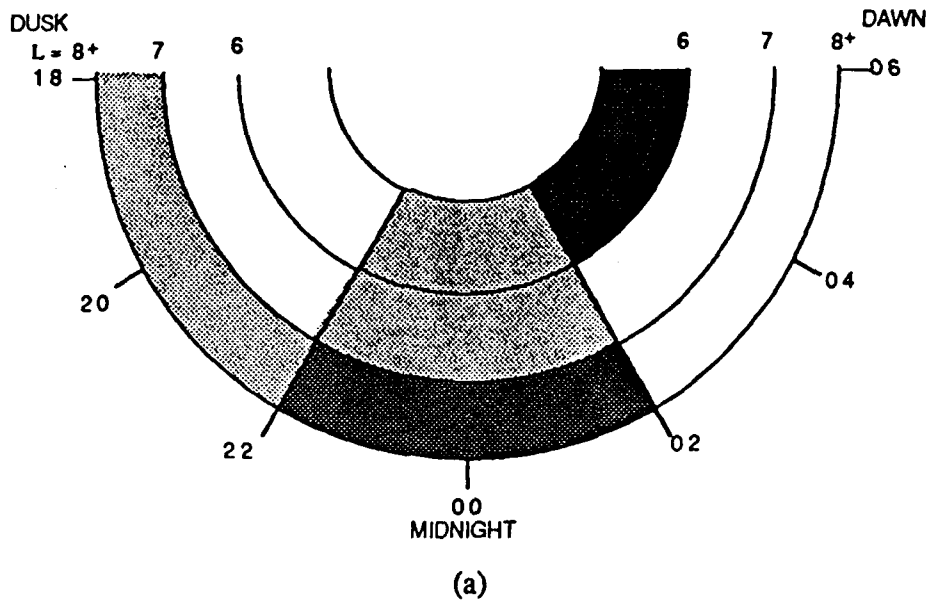# THEORETICAL DIFFUSION OF 1.09KEV ELECTRONS



(a)



(b)

Figure 5-9. (a) Estimated diffusion of quiet time 1.09keV electrons whose anisotropy is given in (b).

Table 5-3. ECH wave amplitudes.

| CASE | LOCAL TIME (MAG) | L VALUE | ELECTRON (keV) | $R_{BIN}$ | R | $R_{DECON}$ | $K_{TH}$ (keV) | $<D_{\alpha\alpha}>$ x10$^{-3}$ | $D_{\alpha\alpha}$ x10$^{-4}$ | ECH AMP (mV/m) |
|---|---|---|---|---|---|---|---|---|---|---|
| 1 | 1800-2200 | 5 | 19.4 | 1.78 | 1.78 | 1.40 | 1.4 | 2.0 | 0.1 | 17.8 |
| 2 | 2200-0200 | 5 | 19.4 | 1.95 | 1.96 | 1.24 | 0.9 | 2.0 | 0.06 | 18.9 |
| 3 | 0200-0600 | 5 | 19.4 | 2.82 | 2.70 | 1.64 | 0.4 | 5.0 | 0.02 | 21.4 |
| 4 | 1800-2200 | 6 | 19.4 | 1.88 | 1.85 | 1.35 | 0.3 | 1.9 | 0.005 | 32.1 |
| 5 | 2200-0200 | 6 | 19.4 | 2.03 | 2.04 | 1.42 | 0.5 | 0.2 | 0.04 | 5.2 |
| 6 | 0200-0600 | 6 | 19.4 | 3.20 | 3.44 | 2.67 | 0.8 | 0.2 | 0.05 | 5.9 |
| 7 | 1800-2200 | 7 | 19.4 | 1.86 | 1.85 | 1.35 | 0.6 | 1.8 | 0.04 | 16.2 |
| 8 | 2200-0200 | 7 | 19.4 | 2.05 | 2.08 | 1.79 | 1.8 | 1.5 | 0.1 | 16.1 |
| 9 | 2200-0200 | 6 | 19.4 | 2.03 | 2.70 | 1.75 | 0.8 | 0.2 | 0.05 | 5.5 |
| 10 | 2200-0200 | 6 | 19.4 | 2.03 | 1.17 | 0.95 | 1.6 | 2.0 | 0.1 | 18.5 |
| 11 | 2200-0200 | 5 | 4.52 | 2.51 | 2.69 | 2.30 | 0.7 | 0.1 | 0.2 | 2.2 |
| 12 | 0200-0600 | 5 | 4.52 | 2.97 | 2.69 | 1.85 | 1.1 | 0.1 | 0.6 | 1.6 |
| 13 | 2200-0200 | 6 | 4.52 | 2.26 | 2.54 | 2.21 | 1.3 | 0.1 | 0.9 | 1.3 |
| 14 | 0200-0600 | 6 | 4.52 | 2.93 | 2.80 | 1.85 | 0.7 | 1.1 | 0.2 | 6.1 |
| 15 | 1800-2200 | 7 | 4.52 | 2.49 | 2.70 | 2.21 | 1.0 | 1.0 | 0.6 | 4.2 |
| 16 | 2200-0200 | 7 | 4.52 | 2.13 | 2.21 | 1.46 | 1.1 | 0.9 | 0.6 | 4.2 |
| 17 | 0200-0600 | 6 | 4.52 | 2.97 | 1.22 | 1.04 | 1.0 | 1.3 | 0.4 | 5.5 |
| 18 | 2200-0200 | 5 | 1.09 | 2.48 | 2.30 | 1.69 | 1.5 | 0.06 | 2.0 | 0.48 |
| 19 | 0200-0600 | 5 | 1.09 | 2.25 | 1.85 | 1.48 | 1.0 | 0.7 | 10.0 | 0.88 |
| 20 | 2200-0200 | 6 | 1.09 | 3.80 | 2.54 | 1.65 | 1.3 | 0.06 | 10.0 | 0.28 |
| 21 | 1800-2200 | 7 | 1.09 | 2.24 | 2.21 | 1.77 | 1.0 | 0.5 | 7.0 | 0.85 |
| 22 | 2200-0200 | 7 | 1.09 | 1.69 | 1.46 | 1.19 | 1.1 | 0.4 | 10.0 | 0.72 |
| 23 | 2200-0200 | 6 | 1.09 | 2.19 | 1.00 | 1.04 | 1.0 | 6.2 | 9.0 | 0.81 |

$R$ - $J_{\perp}/J_{\parallel}$
$R_{BIN}$ - bin average R
$R_{DECON}$ - deconvolved R
$K_{TH}$ - thermal energy
$<D_{\alpha\alpha}>$ - diffusion coefficient
$D_{\alpha\alpha}$ - normalized diffusion coefficient
ECH AMP - ECH wave amplitude

$$|E_w|_o^2 = \langle D_{\alpha\alpha} \rangle \frac{K_{th}}{\mathcal{D}_{\alpha\alpha}(\alpha_o, K/K_{th})} \qquad (5\text{-}10)$$

recall $|E_w|_o$ is the equatorial ECH wave amplitude, $\langle D_{\alpha\alpha} \rangle$ is the bounce averaged diffusion coefficient, K is the particle energy, $K_{th}$ is the thermal energy, and $\mathcal{D}_{\alpha\alpha}(\alpha_o, K/K_{th})$ is the normalized pitch angle diffusion coefficient.

The values for $\mathcal{D}_{\alpha\alpha}$ were available from the calculations of Lyons [1974]. The thermal energy $K_{th}$ (actually, the average energy) was derived using an algorithm which integrates the entire 21 channel energy distribution in a three dimensional model. This requires an assumption of symmetry about the parallel axis [Croley, personal communications, 1990]. The thermal energies used in (5-10) were an average of $K_{th_\perp}$ and $K_{th_\parallel}$. In Lyons [1974], $K_{th_\perp}$ and $K_{th_\parallel}$ were considered equal. The case to case variation of $K_{th}$ in the 19.4keV sample cases were large, $K_{th} = 0.83 \pm 0.52$. Much smaller case to case variations of thermal energy were noted in the sample cases used for 4.52 and 1.09keV; $K_{th} = 0.99 \pm 0.2$ and $1.1 \pm 0.2$, respectively.

The bounce averaged diffusion coefficient $\langle D_{\alpha\alpha} \rangle$ was derived from the results of the fit performed to determine the strength of the diffusion. The minimum lifetime $\tau_m$ (3-43) was factored out of the diffusion coefficient obtained from Figure 3-2 so that $\langle D_{\alpha\alpha} \rangle = D(0^\circ)$.

The resultant ECH wave amplitudes represent the minimum wave emissions required by the theoretical results of Lyons [1974] to produce a distribution similar to the observed. For the 19.4keV electrons in Table 5-3, the ECH wave amplitudes ranged from 5.2 to 32.1mV/m. Two cases with anisotropies much higher and much lower than the bin average ($R_{BIN}$=2.03) in the midnight sector at $6 \leq L < 7$ were also determined. For a very anisotropic distribution (R=2.70), case 9 on Table 5-3, the required wave amplitude was 5.51mV/m. Case 10 is a nearly isotropic distribution (R=1.17) and would require an amplitude of 18.5mV/m. This change in wave amplitude reflects the greater power case 10

66

requires to isotropize the distribution.

Six cases of average anisotropies were available at the 4.52keV energy level. The estimated wave amplitudes corresponding to these 4.52keV angular distribution are cases 11 through 16 on Table 5-4. They ranged from 1.3 to 6.1mV/m. A nearly isotropic case (R=1.22) in case 17 would be consistent with a 5.5 mV/m wave amplitude. This is a relatively high amplitude and is indicative of the greater power required to fill the loss cone. Wave amplitudes of 0.28 to 0.88mV/m are needed to reproduce the anisotropies of the 1.09keV electron distributions. The wave amplitudes consistent with the anisotropy observed in each local time/L bin are cases 18 through 22 on Table 5-4. The isotropic sample (R=1.00) in case 23, as noted before in similar cases above, would require an relative high amplitude of 0.81mV/m to create the observed distribution.

# CHAPTER 6

# CONCLUSIONS

I have investigated the assumption that electrons in the near earth plasma sheet are on strong diffusion during magnetically quiescent times. This assumption has been invoked in numerous studies of magnetospheric coupling with the diffuse aurora [Fontaine et al., 1985, Fontaine and Blanc, 1983; Kennel and Ashour-Abdalla, 1982; Kennel, 1969; among others]. The assumption of strong diffusion is supported by low altitude observations of isotropy on precipitating electrons causing the diffuse aurora [Winningham, 1975; McDairmid and Budzinski, 1968; Chase, 1968] and isotropy of the plasma sheet electron distributions during geomagnetically active periods [Baker et al., 1981]. In this study, sample pitch angle distributions were selected to represent average electron angular distributions for the quiet time (Kp≤3) plasma sheet. The instrument response was removed from the sample distributions by means of a deconvolution algorithm.

A total of nineteen cases representing average pitch angle anisotropy were examined at three energies (1.09, 4.52, and 19.4keV). None of the cases displayed angular distributions consistent with strong pitch angle diffusion. Moderate to weak diffusion was found exclusively. Examination of a case of nearly isotropic distribution at 19.4 and one at 1.09KeV also were consistent with only moderate diffusion. I thus conclude that electrons in the equatorial near earth plasma sheet are usually not under the influence of strong diffusion when Kp≤3.

The assumption that strong diffusion is required to sustain the diffuse aurora is then unsupported. This lack of strong diffusion is inconsistent with the previously observed isotropic pitch angle distributions in the diffuse aurora. One possible explanation is that a secondary process is acting to isotropize the precipitating electrons at low to middle

68

altitudes. Koons et al. [1972] suggested scattering by extremely low frequency waves observed at altitudes of 2000-4500km might be responsible. Another possibility is that the pitch angle isotropy observed at low altitudes in the diffuse auroral regions is not the predominate distribution during geomagnetically quiet times. A review of low altitude electron data limited to magnetic quiescence is suggested as a follow-up study.

To determine if weak to moderate diffusion evidenced by the results is adequate to create and sustain the diffuse aurora, the flux in the atmospheric loss cone must be checked. This would require a comparison of equatorial electron flux in the loss cone to the precipitating flux in the diffuse aurora. Simultaneous observations from high and low altitude satellites near the same magnetic field line would be required. To derive the flux in the loss cone, either the resolution of particle detectors must be improved or observations must undergo an extensive deconvolution process such as was done in this study. Also, great care must be taken with the magnetic mapping.

The second part of this investigation dealt with the minimum ECH wave amplitudes necessary to create the observed pitch angle distributions. All other possible contributors to the diffusion process were excluded from this study. The resulting wave amplitudes ranged from a quiet time high of 32.1mV/m for the 19.4keV electrons to a low of .28mV/m for 1.09keV electrons. These ECH wave amplitudes are one to three orders of magnitude greater than those observed by Roeder and Koons [1989] and Belmont [1983] (see Table 6-1). These high amplitudes are in agreement with the results of Schumaker et al. [1989] who also derived higher than observed amplitudes from their set of equatorial electron distributions. Recall, the distributions reported here were found to be undergoing only weak to moderate diffusion. If strong diffusion were in effect the derived amplitudes would have been higher by a factor of 3 to 10.

Thus, the conclusion that particle-ECH wave interactions are the primary mechanism diffusing electrons into the loss cone at during quiet times is rejected. The

Table 6-1. Occurrence of ECH wave emissions [From Roeder and Koons, 1989].

| Spacecraft | $L$ | $\lambda_D$, deg | $E_l$, mV m$^{-1}$ | Occurrence |
|---|---|---|---|---|
| GEOS 2 | 6.6 | $-3$ | 0.1 | 0.12 |
| | 6.6 | $-3$ | 1.0 | 0.02 |
| AMPTE IRM | 4–8 | $\pm 10$ | 0.035 | 0.27 |
| | 8–12 | $\pm 10$ | 0.012 | 0.26 |
| SCATHA | 5–8 | $\pm 5$ | 0.016 | 0.45 |

question of what wave-particle interactions or other process is responsible for the continuous diffuse aurora remains unanswered. For lack of any other known semicontinuous source of waves in the equatorial plasma sheet, Roeder and Koons [1989] suggested the possibility that wave-particle interactions at low or middle altitudes on auroral field lines might be responsible for the near pitch angle isotropy observed there in conjunction with the diffuse aurora.

I hope the observations presented here will aid in the continuing search for the elusive mechanism coupling the ionospheric diffuse aurora to the magnetosphere.

# REFERENCES

Ashour-Abdalla, M. and Thorne, R. M., Toward a unified view of diffuse auroral precipitation, J. Geophys. Res., 83, 4755-4766, 1978.

Baker, D. N., P. Stauning, E. W. Hones, Jr., P. R. Higbie, and R. D. Belian, Near-equatorial, high-resolution measurements of electron precipitation at L~6.6, J. Geophys. Res., 86, 2295-2313, 1981.

Belmont, G., D. Fontaine,and P. Canu, Are equatorial cyclotron waves responsible for diffuse auroral electron precipitation?, J. Geophys. Res., 88, 9163-9170, 1983.

Canu, P., Etude des ondes électrostatiques à l'aide du satellite GEOS-2, Thèsis, Pierre & Marie Curie University, Paris, France, 1982.

Chase, L. M., spectral measurements of auroral zome particles, J. Geophys. Res., 73, 3469-3478, 1968.

Chen, F. F., Introduction to Plasma Physics and Controlled Fusion, Vol. 1: Plasma Physics. Plenum Press, New York, 1988.

Cornwall, J. M., and M. Schulz, Electromagnetic ion cyclotron instabilities in multicomponent magnetospheric plasmas, J. Geophys. Res., 76, 7791-7796, 1971.

Croley, D. R., personal communications, 1990.

Eather, R. H., S. B. Mende, and R. J. R. Judge, Plasma injection at synchronous orbit and spatial and temporal auroral morphology, J. Geophys. Res., 81, 2805-2824, 1976.

Ejiri, M., Trajectory traces of charged particles in the magnetosphere, J. Geophys. Res., 83, 4798-4810, 1978.

Fairfield, D. H., and Viñas, A. F., The inner edge of the plasma sheet and the diffuse aurora, J. Geophys. Res., 89, 841-954, 1984.

Fennell, J. F., Description of P78-2 (SCATHA) satellite and experiments, in The IMS Source Book, edited by C. T. Russell and D. J. Southwood, 65-81, AGU, Washington D. C., 1982.

Fontaine, D., and M. Blanc, A theoretical approach to the morphology and the dynamics of diffuse auroral zones, J. Geophys. Res., 88, 7171-7184,1983.

Fontaine, D., M. Blanc, L. Reinhart, and R. Glowinsli, Numerical simulations of the magnetospheric convection including the effects of electron precipitation, J. Geophys. Res., 90, 8343-8360, 1985.

Fredericks, R. W., and F. L. Scarf, Recent studies of magnetospheric electric field emission above the electron gyrofrequency, J. Geophys. Res., 78, 310-314, 1973.

Gough, M. P., P. J. Christiansen, G. Martelli, E. J. Gershuny, Interaction of electrostatic waves with warm electrons at the geomagnetic equator, Nature, 279, 515-517, 1979.

Gough, M. P., P. J. Christiansen, and E. J. Gershuny, ES wave morphology near the geostationary orbit, Adv. Space Res., 1, 337, 1981.

Gurnett, D. A., and L. A. Frank, A region of intense plasma wave turbulence on auroral field lines, J. Geophys. Res., 82, 1031-1050, 1977.

Gussenhoven, M. S., D. A. Hardy, and W. J. Burke, DMSP/F2 electron observations of equatorward auroral boundaries and their relationship to magnetospheric electric fields, J. Geophys. Res., 86, 768-778, 1981.

Gussenhoven, M. S., D. A. Hardy, and N. Heinemenn, Systematics of the equatorward diffuse auroral boundary, J. Geophys. Res., 88, 5692-5708, 1983.

Hardy, D. A., M. S. Gussenhoven, and E. Holeman, A statistical model of auroral electron precipitation, J. Geophys. Res., 90, 4229-4248, 1985.

Hoffman, R. A., and J. L. Burch, Electron precipitation patterns and substorm morphology, J. Geophys. Res., 79, 2867-2884, 1973.

Horwitz, J. L., W. K. Cobb, C. R. Baugher, C. R. Chappell, L. A. Frank, T. E. Eastman, R. R. Anderson, E. G. Shelley, and D. T. Young, On the relationship of the plasmapause to the equatorward boundary of the auroral oval and to the inner edge of the plasma sheet, J. Geophys. Res., 87, 9059-9069, 1982.

Kennel, C. F., and F. Engelmann, Velocity space diffusion from weak plasma turbulence in a magnetic field, Phys Fluids, 9, 2377-2388, 1966.

Kennel, C. F., and H. E. Petcshek, Limit on stably trapped particles fluxes, J. Geophys. Res., 71, 1-28, 1966.

Kennel, C. F., Consequences of a magnetospheric plasma, J. Geophys. Res., 7, 379-419, 1969.

Kennel, C. F., F. L. Scarf, R. W. Fredericks, J. H. McGehee and F. V. Coroniti, VLF electron field observation in the magnetosphere, J. Geophys. Res., 75, 6136-6152, 1970.

Kennel, C. F., and M. Ashour-Abdalla, Electrostatic waves and the strong diffusion of magnetospheric electrons, in Magnetospheric Plasma Physics, edited by A. Nishida, 245-344, D. Reidel, Hingham, Mass., 1982.

Kivelson, M. G., and S. J. Southwood, Approximations for the study of drift boundaries in the magnetosphere, J. Geophys. Res., 80, 3528-3534, 1975.

Koons, H. C., A. L. Vampola, and D. A. McPherson, Strong pitch angle scattering of energetic electrons in the presence of electrostatic waves above the ionospheric trough region, J. Geophys. Res., 77, 1771-1775, 1972.

Lui, A. T. Y., and C. D. Anger, A uniform belt of diffuse auroral emission seen by the ISIS-2 scanning photometer, Planet. Space Sci., 21, 799-809, 1973.

Lui, A. T. Y., D. Venkatesan, C. D. Anger, S.-I. Akasofu, W. J. Heikkila, J. D. Winningham, and J. R. Burrows, Simultaneous observations of particle precipitations and auroral emissions by the Isis 2 satellite in the 19-24 MLT sector, J. Geophys. Res., 82, 2210-2228, 1977.

Lyons, L. R., R. M. Thorne, and C. F. Kennel, Pitch-angle diffusion of radiation belt electrons within the plasmasphere, J. Geophys. Res., 77, 3455-3474, 1972.

Lyons, L. R., Comments on pitch angle diffusion in the Radiation Belts, J. Geophys. Res., 78,6793-6797, 1973.

Lyons, L. R., Electron diffusion driven by magnetospheric electrostatic waves, J. Geophys. Res., 79, 575-580, 1974.

Lyons, L. R., and D. J. Williams, Quantitative Aspects of Magnetospheric Physics. Reidel, Boston, 1984.

Lyons, L. R., and J. F. Fennell, Characteristics of auroral electron precipitation on the morningside, J. Geophys. Res., 91, 11,225-11,234, 1986.

Lyons, L. R., personal communications, 1990.

McDiarmid, I. B., and E. E. Budzinski, B. A. Search for low-altitude acceleration mechanisms during an auroral substorm, Can. J. Phys., 46, 941-912, 1968.

McIlwain, C. E., Coordinates for mapping the distribution of magnetically trapped particles, J. Geophys. Res., 66, 3681, 1961.

McIlwain, C. E., Auroral electron beams near the magnetic equator, in Nobel Symposium Proceedings, Plenum Press, London, 1975.

Mende, S. B., and Eather, T. H., Monochromatic all-sky observations and auroral precipitation patterns, J. Geophys. Res., 81, 3771-3780, 1976.

Meng, C. I., B. Mauk and C. E. McIlwain, Electron precipitation of evening diffuse aurora and its conjugate electron fluxes near the magnetospheric equator, J. Geophys. Res., 84, 2545-2558, 1979.

Newell, P. T., and C.-I. Meng, Energy dependence of the equatorward cutoffs in auroral electron and ion precipitation, J. Geophys. Res., 92, 7519-7530, 1987.

O'Brien, B. J., High-latitude geophysical studies with satellite Injun 3, Precipitation of electrons into the atmosphere, J. Geophys. Res., 69, 13-44, 1964.

Olson, W. P., and K. A. Pfitzer, A quantitative model of the magnetospheric magnetic field, J. Geophys. Res., 79, 3739-3748, 1974.

Roberts, C. S., Pitch angle diffusion of electrons in the magnetosphere, Rev. Geophys Space Phys., 7, 305-338, 1969.

Roeder, J. L., and D. J. Gorney, Restoration of particle pitch angle distribution functions by maximum entropy algorithm, Aerospace Report No. ATR-86(7098)-3, 1986.

Roeder, J. L., H. C. Koons, A survey of electron cyclotron waves in the magnetosphere and the diffuse auroral electron precipitation, J. Geophys. Res., 94, 2529-2541, 1989.

Roederer, J., Dynamics of Geomagnetically Trapped Radiation, Springer-Verlag, New York, 1970.

Schumaker, T. L., M. S. Gussenhoven, D. A. Hardy, and R. L. Carovillano, The relationship between diffuse auroral and plasma sheet electron distribution near local midnight, J. Geophys. Res., 94, 10,061-10,078, 1989.

Schulz, M., and L. J. Lanzerotti, Particle Diffusion in the Radiation Belts, Springer, New York, 1973.

Slater, D. W., L. L. Smith, and E. W. Klechner, Correlated observations of the

equator ward diffuse auroral boundary, J. Geophys. Res., 85, 531-542, 1980.

Southwood, D. J., and S. M. Kaye, Drift boundary approximations in simple magnetospheric convection models, J. Geophys. Res., 84, 5773-5780, 1979.

Stevens, J. R., A. L. Vampola, Description of the space test program P78-2 spacecraft and payloads, SAMSO TR-78-24 (now Space Division), USAF, 1978.

Taylor, J. R., An Introduction to Error Analysis. Oxford University Press, London, 1982.

Thorne, R. M., As-240B Class Notes, 100-114 , 1989.

Whalen, J. A., The aurora, in A. S. Jursa (Ed.), Handbook of Geophysics and Space Environment, 12.1, Air Force Geophysics Laboratory, Boston, 1985.

Winningham, J. D., F. Yasuhara, S.-I, Akasofu, and W. J. Heikkila, The latitudinal morphology of 10eV to 10keV electron fluxes during magnetically quiet and disturbed times in the 2100-0300 MLT sector, J. Geophys. Res., 80, 3148-3171, 1975.